

# Climate, Oxygen, and the Future of Marine Biodiversity

Curtis Deutsch,<sup>1,2</sup> Justin L. Penn,<sup>1</sup> and Noelle Lucey<sup>2,3</sup>

<sup>1</sup>Department of Geosciences, Princeton University, Princeton, New Jersey, USA;  
email: cdeutsch@princeton.edu

<sup>2</sup>High Meadows Environmental Institute, Princeton University, Princeton, New Jersey, USA

<sup>3</sup>Smithsonian Tropical Research Institute, Balboa Ancón, Panama

Annu. Rev. Mar. Sci. 2024. 16:217–45

First published as a Review in Advance on  
September 14, 2023

The *Annual Review of Marine Science* is online at  
[marine.annualreviews.org](https://marine.annualreviews.org)

<https://doi.org/10.1146/annurev-marine-040323-095231>

Copyright © 2024 by the author(s). This work is licensed under a Creative Commons Attribution 4.0 International License, which permits unrestricted use, distribution, and reproduction in any medium, provided the original author and source are credited. See credit lines of images or other third-party material in this article for license information.

## Keywords

climate change, hypoxia, biodiversity, marine species, deoxygenation, ecosystem

## Abstract

The ocean enabled the diversification of life on Earth by adding O<sub>2</sub> to the atmosphere, yet marine species remain most subject to O<sub>2</sub> limitation. Human industrialization is intensifying the aerobic challenges to marine ecosystems by depleting the ocean's O<sub>2</sub> inventory through the global addition of heat and local addition of nutrients. Historical observations reveal an ~2% decline in upper-ocean O<sub>2</sub> and accelerating reports of coastal mass mortality events. The dynamic balance of O<sub>2</sub> supply and demand provides a unifying framework for understanding these phenomena across scales from the global ocean to individual organisms. Using this framework, we synthesize recent advances in forecasting O<sub>2</sub> loss and its impacts on marine biogeography, biodiversity, and biogeochemistry. We also highlight three outstanding uncertainties: how long-term global climate change intensifies ocean weather events in which simultaneous heat and hypoxia create metabolic storms, how differential species O<sub>2</sub> sensitivities alter the structure of ecological communities, and how global O<sub>2</sub> loss intersects with coastal eutrophication. Projecting these interacting impacts on future marine ecosystems requires integration of climate dynamics, biogeochemistry, physiology, and ecology, evaluated with an eye on Earth history. Reducing global and local impacts of warming and O<sub>2</sub> loss will be essential if humankind is to preserve the health and biodiversity of the future ocean.

ANNUAL  
REVIEWS **CONNECT**

[www.annualreviews.org](https://www.annualreviews.org)

- Download figures
- Navigate cited references
- Keyword search
- Explore related articles
- Share via email or social media



## 1. INTRODUCTION

Oxygen is fundamental to life on Earth. The ocean is responsible for the rise of atmospheric O<sub>2</sub> that brought about the transition from a microbial ocean to the rich animal diversity seen today, from tropical coral reefs to temperate kelp forests and the dark mesopelagic twilight zone. The oxygenation of the ocean and the diversification of its biota have not been steady, unidirectional processes (Sperling et al. 2022). Ocean O<sub>2</sub> levels have declined many times in geological history, temporarily reversing the long-term trend toward greater species richness.

Industrial societies have become a geological force (Lewis & Maslin 2015), causing unprecedented rates of biomass extraction and habitat destruction. We are also altering the global energy balance of Earth's climate (IPCC 2021), the nutrient balance of the biosphere (Battye et al. 2017), and, as a result, the mass balance of oceanic O<sub>2</sub> (Keeling et al. 2010). These global changes collectively accentuate the unique and preexisting aerobic challenge to life in the sea (Seibel 2011) and threaten a sixth mass extinction (Penn & Deutsch 2022).

The persistent role of O<sub>2</sub> in limiting habitability in the sea but not on land arises from fundamental physical differences between the atmosphere and ocean. The ocean retains <2% of the global O<sub>2</sub> inventory, while the other >98% resides in the atmosphere. The partition of O<sub>2</sub> between the two domains primarily reflects O<sub>2</sub> solubility in seawater ( $K_H$ ) (Sarmiento & Gruber 2006). However, this is not the critical biological difference, as the thermodynamic driving force for O<sub>2</sub> transfer is the O<sub>2</sub> partial pressure ( $p_{O_2}$ ) (atm), which is equilibrated between the surface ocean and atmosphere by rapid air–sea exchange. Instead, the constraining role of O<sub>2</sub> for ocean species arises from two kinematic factors: the vastly lower diffusivity of gases in water than in air and the slower circulation of the ocean than the atmosphere. Solar heating of Earth's surface ensures a rapid convective mixing of O<sub>2</sub> in the atmosphere on a timescale of days to weeks, but it also prevents the buoyant and O<sub>2</sub>-rich surface ocean from following the path of sinking particulate organic matter to the depths of its decomposition. Ocean surface waters, which take years to centuries to circulate through deeper layers, are unable to oxygenate the subsurface ocean fast enough to keep up with the inexorable respiratory consumption by millions of bacteria in every liter of seawater. These dynamics of global ocean O<sub>2</sub> supply and demand, which made the ocean the primary geological engine of Earth's O<sub>2</sub>, also give rise to the strong and persistent subsurface gradients that create and constrain the habitability for marine organisms.

The industrialization of human societies has produced two negative consequences for the ocean's O<sub>2</sub> reservoir. The nutrients mobilized for agriculture are eventually carried to the coastal ocean in rivers, stimulating phytoplankton growth and thus higher respiratory O<sub>2</sub> demand in deeper waters on the continental shelf. Global warming is a more pervasive but less readily visible change, which causes O<sub>2</sub> depletion throughout the ocean, including the most remote biomes on Earth, far from land and deep below the surface (**Figure 1a**). These two driving forces for O<sub>2</sub> depletion interact in the coastal zone, where open ocean waters intersect the highly productive, dynamic, and biodiverse environments of the continental shelf and slope.

Coastal regions make up only 7% of the ocean's area but contain ~15% of its net primary productivity and ~90% of its animal life. Many coastal ecosystems naturally experience low O<sub>2</sub> because of either high biological activity or upwelling of O<sub>2</sub>-depleted waters from the deeper open ocean. Increasing anthropogenic nutrient inputs are exacerbating these conditions and accelerating the occurrence of low O<sub>2</sub> in coastal waters (Breitburg et al. 2018, Diaz & Rosenberg 2008, Fennel & Testa 2019, Pitcher et al. 2021) (**Figure 1a**). These events cause hypoxic stress for marine animals reliant on aerobic metabolism, resulting in a proportional increase in mass mortality events (**Figure 1b**), depletion of fisheries and aquaculture stocks, and loss of foundation and keystone species vital to ecosystem function (**Figure 1c**). The impacts of nutrient inputs to

### O<sub>2</sub> solubility in

seawater ( $K_H$ ): [O<sub>2</sub>] in seawater when in equilibrium with the O<sub>2</sub> pressure in a gas phase, as a function of temperature, pressure, and salinity

### O<sub>2</sub> partial pressure

( $p_{O_2}$ ): the ratio of O<sub>2</sub> concentration to O<sub>2</sub> solubility

### Hypoxia: the

condition wherein O<sub>2</sub> is insufficient to meet metabolic demand, which varies with species and temperature, in contrast to the fixed definition of [O<sub>2</sub>] < 60 μM commonly used in oceanography

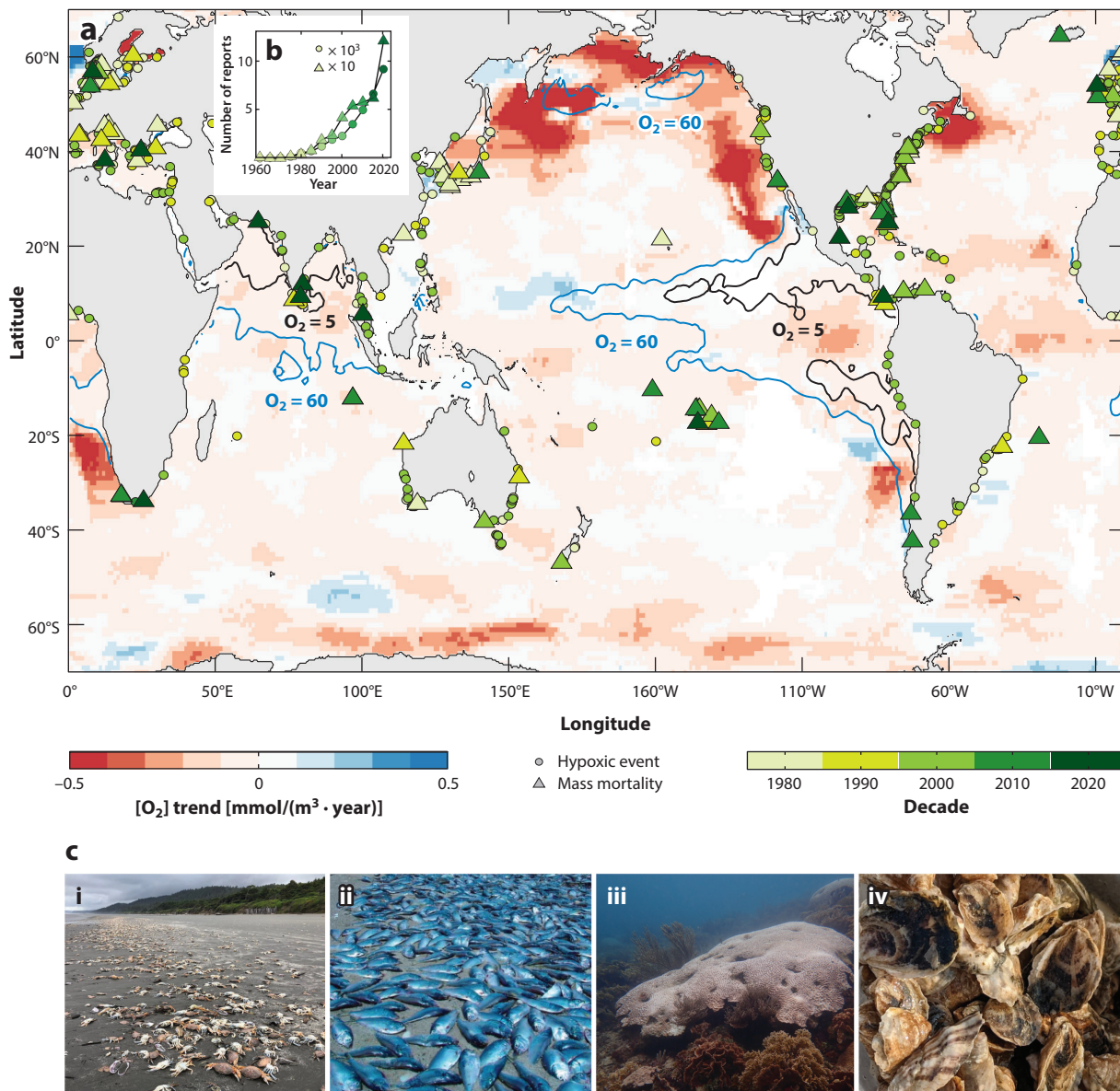


**Figure 1**

Global trends in  $[O_2]$  and the occurrence of extreme hypoxia. (a) Trends in historical  $[O_2]$  over the period 1958–2015 (color field) at 200-m depth overlaid with documented cases of coastal hypoxia that have either been detrimental to marine animals (circles) or resulted in mass mortalities (triangles). Color field adapted from Ito et al. (2017); data for hypoxic events through 2022 updated from Diaz et al. (2011) and Altieri et al. (2017). Contours delineate where the annual mean  $[O_2]$  reaches a vertical minimum in the upper 200 m of  $5 \mu\text{M}$  (black) and  $60 \mu\text{M}$  (blue), thresholds for aerobic function commonly ascribed to microbes and animals, respectively (see Figure 2). (b) Number of reported hypoxic events and mass mortalities plotted by publication year from 1958 through 2022. Hypoxic and mass mortality events in coastal waters have accelerated, with one in every hundred hypoxic events resulting in a mass mortality. (c) Photos showing the diversity of marine animals impacted by  $O_2$ -driven mortality: (i) dead Dungeness crabs from the Pacific Northwest coast of the United States; (ii) dead Menhaden fish washed up on the shores of Rhode Island, United States; (iii) bleached brain coral from the Caribbean coast of Panama; and (iv) dead Eastern oysters. Subpanel i adapted from Marquis (2022) (public domain); subpanel ii by Chris Deacutis/Flickr (<https://www.flickr.com/photos/48722974@N07/4523955644>) (CC BY 2.0); subpanels iii and iv by N. Lucey. For further details on the creation of panels a and b, see Supplemental Appendix A.

**Supplemental Material** >

---

**Eutrophication:**

increased growth, primary production, and biomass of algae in response to nutrient enrichment in the environment (e.g., sewage, fertilizer, and detergents)

**Metabolic storm:**

an anomalous ocean weather event in which high temperatures cause elevated organismal  $O_2$  demand simultaneous with a decline in  $O_2$  available in seawater

**Temperature-dependent hypoxia:**

the threshold for hypoxia and its variation with temperature

**Oxygen minimum zone (OMZ):**

a vertical minimum in water-column  $[O_2]$ ; OMZs are globally prevalent but are strongest in the tropical thermoclines of the Indian and Pacific basins, where  $O_2$  reaches traditionally defined hypoxic concentrations

---

worldwide coastal waters are, or will soon be, amplified by the large-scale  $O_2$  depletion as the signal of climate forcing emerges from natural variability (Andrews et al. 2013, Long et al. 2016) and  $O_2$  trends originating in the open ocean arrive in coastal ecosystems (Buil & Di Lorenzo 2017) that are already experiencing anthropogenic stress (Levin et al. 2015).

Here, we synthesize recent advances in understanding how climate change alters the ocean's  $O_2$  content, exacerbating local coastal eutrophication, with wide-ranging impacts on the distribution and diversity of marine life from microbes to macrofauna. Our emphasis is on the century timescale of historical and future climate change. In light of the notorious difficulty of projecting the future, we focus on understanding that has developed through a close integration of empirical field and laboratory observations with physiological and Earth system models based on first principles. We present these advances through a unifying framework based on the balance of  $O_2$  supply and demand, which provides both a conceptual and quantitative understanding of ocean deoxygenation across multiple scales, from its global causes to its organismal consequences. In seeking robust projections of the ocean's likely future, we also draw heavily on the past, prioritizing conclusions that have been validated against ecosystem responses to climate change observed in the paleo record.

Recent advances also highlight the need for improved understanding related to three key questions of scale. The first involves the distinct timescales of ocean climate and weather: How might long-term global climate change amplify ocean weather in which heatwaves coincide with low  $O_2$  extremes, subjecting organisms to metabolic storms? The second involves multiple scales of biological organization: How will the differential biological sensitivities to temperature-dependent hypoxia seen at a species scale alter the structure of communities at ecosystem scales? Third is the local implications of global change: How do large-scale patterns of open ocean  $O_2$  loss intersect with local coastal nutrient-driven hypoxia and its biological impacts? These three research areas require substantial investment in the further integration of empirical and modeling approaches across historically distinct sectors of the climate, biological, and Earth sciences.

## 2. OCEAN $O_2$ AND CLIMATE, FROM GLOBAL TO ORGANISM SCALES

In the modern ocean,  $O_2$  levels span the full range that has existed on Earth (**Figure 2a**), from the functionally anoxic concentrations that dominated the ancient ocean to  $O_2$  pressures slightly exceeding atmospheric  $pO_2$  at sea level ( $\sim 0.21$  atm). In surface waters,  $O_2$  concentrations ( $\text{mmol}/\text{m}^3$  or  $\mu\text{M}$ ) approximately double from the equator to the pole, paralleling the twofold rise in  $O_2$  solubility in seawater ( $K_H$ ) [ $\text{mol } O_2/(\text{m}^3 \cdot \text{atm})$ ] in accordance with Henry's law,  $pO_2 = O_2/K_H$  (**Table 1** provides a summary of the mathematical symbols used in this review). In waters below the surface mixed layer ( $\sim 50$  m),  $O_2$  concentrations range from near saturation in regions of water-mass formation to depleted values in regions of upwelling, especially in the tropics, eastern boundaries, and the subarctic Pacific. By volume, the most common  $O_2$  levels are the intermediate concentrations found at thermocline depths (100–1,000 m) of the large subtropical gyres of all major basins (**Figure 2b**).

The  $O_2$  throughout most of the ocean is well in excess of lethal levels measured for most animal species (**Figure 2c**). Such data have historically been used to define a single hypoxic threshold of  $\sim 60$   $\mu\text{M}$  (2 mg/L) (Vaquer-Sunyer & Duarte 2008), encompassing much of the vertical oxygen minimum zones (OMZs) of all basins (Paulmier & Ruiz-Pino 2009, Karstensen et al. 2008). However, coarse averages of extreme thresholds can obscure the wide interspecific variation and the more pervasive sublethal effects on animal behavior, ecological fitness, and geographic range, as well as interactions between  $O_2$  and other stressors, such as temperature. Maintenance of minimal metabolic rate requires slightly higher  $O_2$  (**Figure 2c**), but this criterion still underestimates

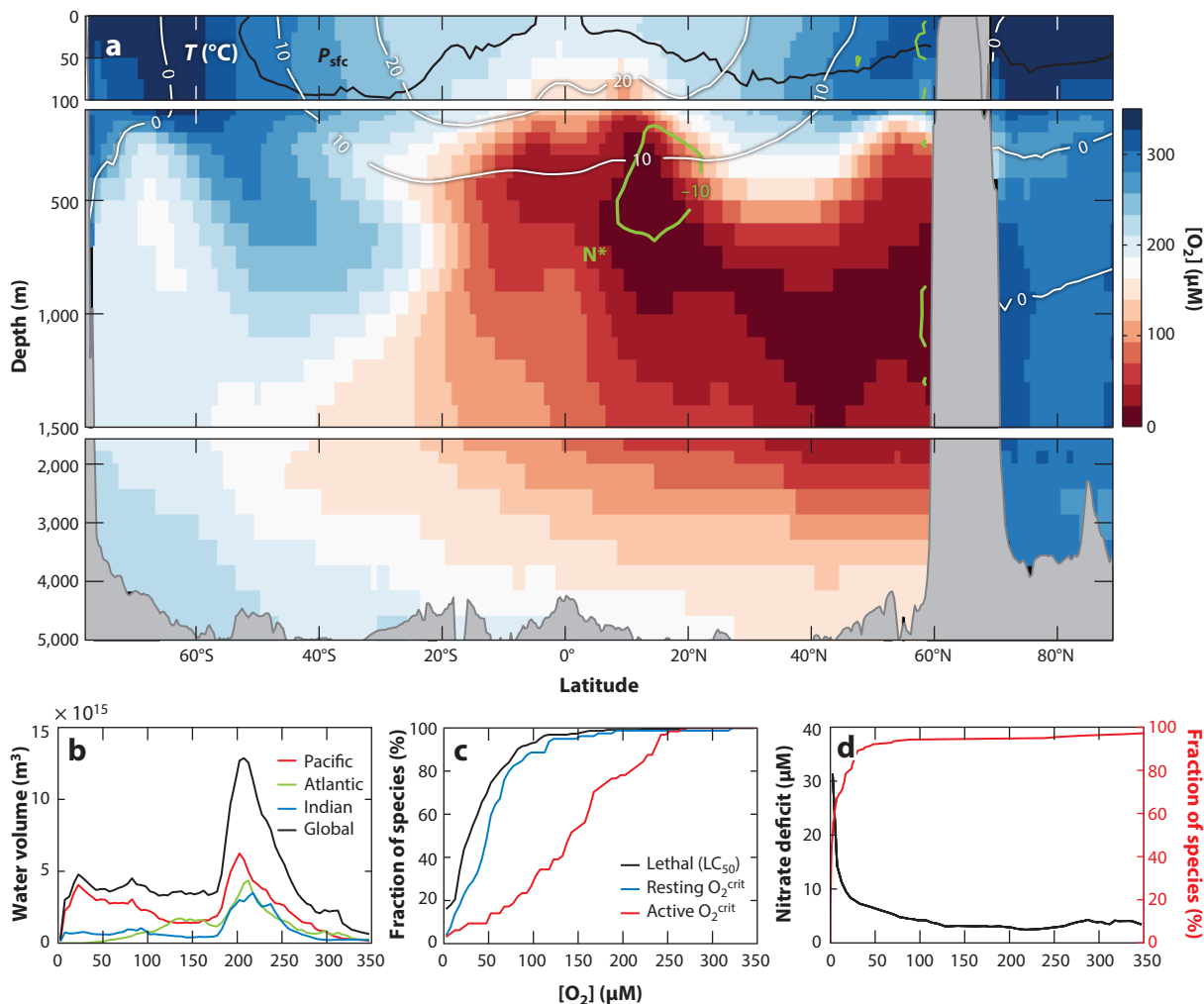


**Figure 2**

Spatial and volumetric distributions of  $O_2$  and frequency distributions of biological  $O_2$  thresholds. (a) Climatological observations of  $[O_2]$  (color) versus depth and latitude in the eastern Pacific (160–70°W, zonal average) overlaid with temperature (white lines) and the deficit of nitrate concentration ( $[NO_3^-]$ ) relative to phosphate concentration ( $[PO_4^{3-}]$ ),  $N^* = [NO_3^-] - 16 \cdot [PO_4^{3-}]$ , caused by microbial nitrogen loss (green contour =  $-10$   $\mu M$ ) in suboxic conditions ( $[O_2] < 5$   $\mu M$ ) in the water column or sediment. The contour in the surface layer traces where  $pO_2$  is at equilibrium with the atmosphere ( $P_{sfc}$ ; black line). (b) Global water volume (0–1,000 m) at each  $[O_2]$ . (c) Cumulative fraction of animal species with  $O_2$  thresholds for mortality ( $LC_{50}$ ) (Vaquer-Sunyer & Duarte 2008) and metabolism ( $O_2^{crit}$ ) in resting and active states (Deutsch et al. 2020). (d) Mean ocean  $N^*$  versus  $[O_2]$  (black line) and cumulative fraction of aerobic microbe species that can respire aerobically at each  $[O_2]$  level, measured as the half-saturation for whole-cell uptake rate (red line). As  $[O_2]$  approaches suboxic levels, the number of active aerobes declines, while the nitrate deficit from anaerobic microbes rises (Giovannoni et al. 2021). Hydrographic data in all panels are from climatological observations (Boyer et al. 2018). Abbreviation:  $pO_2$ ,  $O_2$  partial pressure.

ecologically relevant thresholds severalfold. When either metric is elevated by a factor of  $\sim 3$  to account for sustained ecological activity (Hammond & Diamond 1997), species thresholds closely match ocean conditions, a first hint that ocean  $O_2$  distribution may be routinely and broadly limiting to marine animals.



Table 1 Definitions of mathematical symbols used in this review

Symbol	Definition
$A_c$	Species active hypoxia tolerance (1/atm), equivalent to the resting hypoxia tolerance divided by the ratio of active to resting metabolic rates ( $A_c = A_o / \Phi_{crit}$ )
$A_o$	Species resting hypoxia tolerance (1/atm) or the ratio of O <sub>2</sub> supply ( $\alpha_S$ ) to demand ( $\alpha_D$ ), measurable as $1/pO_2^{crit}$ at a reference temperature ( $T_{ref}$ ) and body size ( $B_{ref}$ )
$Ar(E,T)$	The Arrhenius exponential factor (unitless), which describes how biological rates and $pO_2^{crit}$ vary with temperature and is equal to $\exp[\frac{-E}{k_B}(\frac{1}{T} - \frac{1}{T_{ref}})]$ , where $E$ is the temperature sensitivity, $k_B$ is Boltzmann's constant, and $T_{ref}$ is the reference temperature
$B$	Organism body mass (unitless) relative to a reference body size ( $B_{ref}$ )
$E_o$	The temperature sensitivity of hypoxia tolerance (eV), equal to the difference between the temperature sensitivity of metabolic demand ( $E_d$ ) and O <sub>2</sub> supply ( $E_s$ ) and measurable from the slope of $\ln(pO_2^{crit})$ versus $1/k_B T$
$E_d$	The temperature sensitivity of metabolic rate (eV)
$E_s$	The temperature sensitivity of O <sub>2</sub> supply (eV), calculated from $E_s = E_d - E_o$
$R_o$	The rate of metabolic O <sub>2</sub> demand [mol O <sub>2</sub> per unit volume (or body mass) per time], which varies with $T$ and $B$
$R_w$	The rate of respiratory O <sub>2</sub> consumption from seawater [mol O <sub>2</sub> /(m <sup>3</sup> ·time)] from biological demand, equivalent to the average rate that O <sub>2</sub> is depleted along its transport pathway from the surface to the interior ocean
$T$	Temperature (K in all equations)
$\alpha_D$	The metabolic rate (mol O <sub>2</sub> per unit body mass per time) at a reference temperature and body size
$\alpha_S$	The O <sub>2</sub> supply coefficient (mol O <sub>2</sub> per unit body mass per time per atmosphere) at a reference temperature and body size, calculated from $\alpha_S = A_o \cdot \alpha_D$
$\varepsilon$	The allometric scaling exponent of hypoxia tolerance (unitless), equal to the allometric scaling of O <sub>2</sub> supply ( $\sigma$ ) minus the allometric scaling of O <sub>2</sub> demand ( $\delta$ )
$\sigma$	The allometric scaling of organismal O <sub>2</sub> supply (unitless)
$\delta$	The allometric scaling of metabolic O <sub>2</sub> demand (unitless)
$\Psi_o$	The rate coefficient for the physiological O <sub>2</sub> supply (1/time), which incorporates multiple processes, including diffusive fluxes, external ventilation, and internal circulation, into a single effective inverse timescale
$\Psi_w$	The rate coefficient for the physical O <sub>2</sub> supply (1/time) by ocean mixing and circulation, which can be characterized by an inverse timescale (a volumetric flow rate per unit water volume)
$\Phi_{crit}$	The species-specific minimum $\Phi$ threshold (unitless) required to support a long-term population in the environment, corresponding to the ratio of sustained rates of activity to resting metabolism

**Suboxia:** [O<sub>2</sub>] < 5 μM, corresponding to the appearance of nitrogen deficits relative to phosphorus in seawater and the activation of anaerobic microbial metabolisms; used interchangeably with anoxia in this review

At the extreme end of the O<sub>2</sub> scale, the ocean's anoxic and suboxic zones (O<sub>2</sub> < 5 μM) occupy ~0.1% of its total volume. These regions are inhospitable to nearly all marine animals, and even to most aerobic bacteria (Giovannoni et al. 2021), but are a primary habitat for anaerobic microbes whose respiration converts bioavailable N, a key macronutrient and the next most energetically favorable oxidant after O<sub>2</sub>, to inert N<sub>2</sub> gas (Zhang et al. 2020). Although the microbial removal of N is likely initiated only at near-anoxic conditions at the cellular scale (Zakem & Follows 2017) (**Figure 2d**), it can occur in sediment pore waters or marine particles overlain or surrounded by seawater at much higher O<sub>2</sub> levels (Bianchi et al. 2018, Bohlen et al. 2012). The N removal from anoxic zones, evident in the deficit of nitrate (NO<sub>3</sub><sup>-</sup>) relative to phosphate (PO<sub>4</sub><sup>3-</sup>), extends well beyond strictly anoxic waters. Anaerobic microbial processes thus play a critical role in the regulation of global nutrient inventories (Weber & Deutsch 2012) and the limitation of global primary production, especially in low latitudes.

The balance of O<sub>2</sub> supply and demand at oceanic and organismal scales yields simple but powerful expressions that relate  $pO_2$  to both oceanic and organismal dynamics and thus provides a

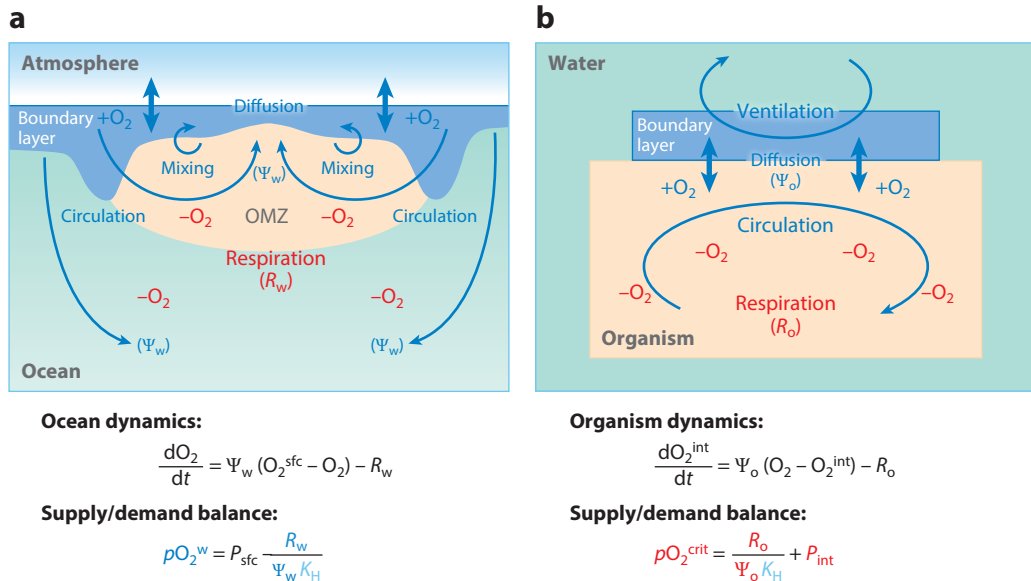


**Figure 3**

Schematic depiction of the mechanisms linking  $O_2$  supply and demand across scales, from (a) the global ocean to (b) individual organisms. In the diagrams, blue and red labels denote sources and sinks of  $O_2$ , respectively; in the underlying equations, blue and red terms denote factors that increase and decrease with temperature, respectively. The rates of respiratory  $O_2$  consumption by oceanic metabolism ( $R_w$ , primarily microbial) and individual animals ( $R_o$ ) and the net effective rate (inverse timescale) of corresponding geophysical and biophysical  $O_2$  transport ( $\Psi_w$  and  $\Psi_o$ , respectively) characterize the rates of  $O_2$  demand and supply for each system, whose linear dynamics and balanced states are given by the equations shown in the lower boxes and used in the main text (Equations 1 and 2). The response of  $pO_2$  and its drivers typically increase (red text) or decrease (blue text) in a warmer ocean as discussed in the main text. Abbreviations: OMZ, oxygen minimum zone;  $pO_2$ ,  $O_2$  partial pressure.

unifying conceptual and quantitative framework for understanding the ocean's  $O_2$  distribution, its spatiotemporal changes with climate, and the response of marine organisms to those changes, including the loss of organism fitness and habitability (Figure 3).

The ocean's  $O_2$  cycle is defined by photosynthetic production, respiratory consumption, and physical transport and air–sea exchange (Figure 3a). Dissolved  $O_2$  enters the surface boundary layer through diffusion across the air–sea interface and photosynthesis in the photic zone. The vast majority of the ocean, the aphotic zone, experiences respiratory  $O_2$  loss, primarily by aerobic microbes. The global biological rates of net surface  $O_2$  production and subsurface consumption are maintained in an extremely close balance by physical processes, from turbulent mixing to basin-scale overturning circulations, which collectively transport  $O_2$  from its producers (phytoplankton) to consumers (animals and heterotrophic microbes). Recasting the  $O_2$  balance well known in oceanography (see Supplemental Appendix B) shows that the  $pO_2$  found along any oceanic flow path is related to the underlying rate of circulation ( $\Psi_w$ ; 1/time) that supplies  $O_2$  from surface waters on a timescale of  $1/\Psi_w$  and the average rate of respiratory demand [ $R_w$ ; mol/( $m^3 \cdot$ time)] that consumes  $O_2$  along that path:

$$pO_2^w = P_{sfc} - \frac{R_w}{\Psi_w K_H}, \quad 1.$$

where the  $O_2$  pressure of surface water,  $P_{sfc}$ , is approximately equal to that of the surface atmosphere. The quantity  $R_w/\Psi_w$  represents the ratio of the rate of  $O_2$  demand to the rate coefficient for its supply and is equivalent to the apparent  $O_2$  utilization (AOU) (mmol/ $m^3$  or  $\mu M$ ) commonly

**Supplemental Material** >

**Apparent  $O_2$  utilization (AOU):** the amount of  $O_2$  consumed by respiration over the transport time of a water parcel from the surface ocean to the interior

Critical O<sub>2</sub> pressure in seawater ( $pO_2^{\text{crit}}$ ): the ambient  $pO_2$  when an organism's O<sub>2</sub> supply balances its resting metabolic O<sub>2</sub> demand

estimated in analysis of observations and models (e.g., Keeling et al. 2010, Long et al. 2019). The solubility converts the O<sub>2</sub> supply rate from concentration to pressure units.

This relationship between  $pO_2$  and the ratio of physical supply and biological demand (Equation 1) can be applied to any water parcel in the ocean interior and can thus explain the mean distribution of  $pO_2$  and its response to climate change. For example, the vertical profile of O<sub>2</sub> and associated depth of OMZs can be predicted from the ratio of vertically declining respiration rates of settling particulate organic matter ( $R_w$ ) versus the rates of circulation ( $\Psi_w$ ). Similarly, the OMZs reach their most extreme intensity in tropical latitudes and in the subarctic North Pacific because waters there have remained away from atmospheric equilibration for the longest, as reflected in ventilation ages (i.e.,  $1/\Psi_w$ ). These critical features of the OMZ constrain animal habitat and create microbial niches for anaerobic removal of bioavailable N.

From an organismal perspective, the global distribution of ambient  $pO_2$  accounts for only half the supply chain (**Figure 3b**). The O<sub>2</sub> available in an organism's environment must be extracted from seawater and transported via a series of biophysical and biochemical mechanisms, analogous to ocean circulation and mixing, to supply the chemical energy of aerobic metabolism at a cellular scale. The O<sub>2</sub> balance at an organism scale yields a parallel relationship (**Figure 3b; Supplemental Appendix B**) between the rate of metabolic demand [ $R_o$ ; mol/(m<sup>3</sup>·time)] and the minimum critical O<sub>2</sub> pressure in seawater ( $pO_2^{\text{crit}}$ , also called  $P_{\text{crit}}$ ) required for a given physiological O<sub>2</sub> supply chain to fuel that demand:

$$pO_2^{\text{crit}} = \frac{R_o}{\Psi_o K_H} + pO_2^{\text{int}}, \quad 2.$$

where  $\Psi_o$  (1/time) is a rate coefficient for the physiological O<sub>2</sub> supply that incorporates multiple processes into a single effective inverse timescale, analogous to that of ocean circulation ( $\Psi_w$ ). The  $pO_2^{\text{crit}}$  is commonly measured in laboratory experiments (e.g., Rogers et al. 2016), and the O<sub>2</sub> pressure of the organism's internal fluid,  $pO_2^{\text{int}}$ , is typically small and neglected.

Similar to the O<sub>2</sub> balance of the global ocean (Equation 1), the organismal O<sub>2</sub> balance (Equation 2) yields fundamental insights into the dynamics of biological O<sub>2</sub> limitation. For example, it predicts that if metabolism ( $R_o$ ) increases faster with temperature than the rates of O<sub>2</sub> supply ( $\Psi_o$ ), then a higher ambient  $pO_2$  will be needed to support that metabolism in warmer water. Similarly, if rates of metabolism rise with growth in body size faster than the O<sub>2</sub> supply, habitability will also require higher  $pO_2$  for larger organisms. While these relationships are qualitatively intuitive, their mathematical expression provides a quantitative framework for deriving less obvious insights, as elaborated below.

That similar expressions could represent O<sub>2</sub> balance at such widely different scales—from the global ocean to a general aquatic organism—reflects the fundamental role that the demand/supply ratio plays in dynamical balances in any system. While their similarity and simplicity are conceptually useful, they are also deceptive, as many layers of complexity lie hidden in the dependence of the organismal rates ( $R_o$  and  $\Psi_o$ ) on physiological processes and in the dependence of the oceanographic rates ( $R_w$  and  $\Psi_w$ ) on climate processes.

The balance between biological O<sub>2</sub> demand and its intricate multiscale global supply chain can also be disrupted by any of those processes, from the metabolism of organisms (including microbes) to the general circulation of the ocean, most of which are sensitive to temperature. These processes and their thermal sensitivities may be diagnosed from observations or predicted from mechanistic dynamical models of the climate system and organismal physiology.

Whether such a simple unifying framework and its component models can make reliable projections for the future of ocean biodiversity ultimately depends on its ability to reproduce observed patterns in the modern ocean and their reconstructed changes in the past. In the following sections, we aim to demonstrate both the framework's utility and its fidelity.

Supplemental Material >



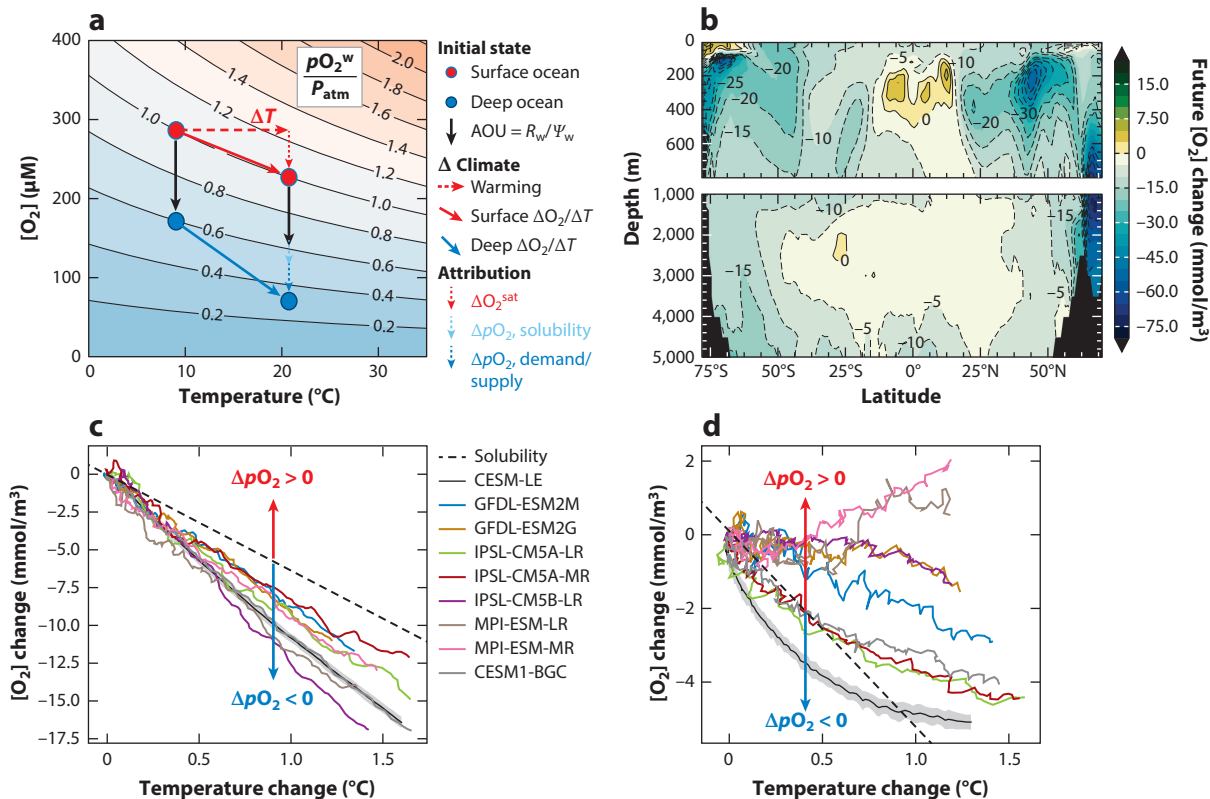


**Figure 4**

Relationship between ocean warming and  $p\text{O}_2$  change in Earth system models. (a) Schematic depiction of the impact of temperature on  $[\text{O}_2]$  (y axis) and  $p\text{O}_2$  (contours) as a fraction of its saturated level ( $P_{\text{atm}}$ ). Ocean warming (dashed red arrow) reduces the saturated  $[\text{O}_2]$  in surface waters via solubility (dotted red arrow) but leaves  $p\text{O}_2$  unchanged (solid red arrow). In deeper waters, where the time-integrated effect of microbial respiration (i.e., AOU) depletes  $\text{O}_2$  below saturated values (black arrows), warming reduces  $p\text{O}_2$  due to nonlinear gas solubility (dotted cyan arrow). Higher AOU, which can arise through either an increased microbial  $\text{O}_2$  demand ( $R_w$ ) or reduced physical  $\text{O}_2$  supply ( $\Psi_w$ ), would further reduce  $p\text{O}_2$  (dotted blue arrow), often exceeding the solubility effect. (b) Projected future  $[\text{O}_2]$  changes averaged over a group of Earth system models (listed in the legend for panels c and d) for the end of this century (relative to 1970) under a high-greenhouse-gas-emissions scenario (RCP8.5). The projected changes show strong spatial variability across depth and latitude. In the tropical thermocline, model mean  $\text{O}_2$  increases in opposition to the global trend. (c,d) Projected changes in  $[\text{O}_2]$  and temperature, averaged over the upper 1,000 m. In each ocean model (colored lines), the change in  $p\text{O}_2$  depends on whether the trajectory of warming and  $[\text{O}_2]$  lies above or below that of solubility (dashed black lines), which depends on whether the  $\text{O}_2$  demand/supply ratio rises or falls (Equation 1). In all models, extratropical  $p\text{O}_2$  declines due to falling  $\text{O}_2$  supply/demand (panel c), whereas tropical  $p\text{O}_2$  rises (panel d), even in models where  $[\text{O}_2]$  decreases. Abbreviations: AOU, apparent  $\text{O}_2$  utilization; CESM-LE, Community Earth System Model, Large Ensemble; CESM1-BGC, Community Earth System Model 1, Biogeochemistry; GFDL-ESM2G, Geophysical Fluid Dynamics Laboratory Earth System Model 2G; GFDL-ESM2M, Geophysical Fluid Dynamics Laboratory Earth System Model 2M; IPSL-CM5A-LR, Institut Pierre Simon Laplace CM5A, Low Resolution; IPSL-CM5B-LR, Institut Pierre Simon Laplace CM5B, Low Resolution; IPSL-CM5A-MR, Institut Pierre Simon Laplace CM5A, Medium Resolution; MPI-ESM-LR, Max Planck Institute Earth System Model, Low Resolution; MPI-ESM-MR, Max Planck Institute Earth System Model, Medium Resolution;  $p\text{O}_2$ ,  $\text{O}_2$  partial pressure; RCP8.5, Representative Concentration Pathway 8.5. Panels b–d adapted from Long et al. (2019).

## 2.1. $\text{O}_2$ Supply and Demand at the Ocean Scale

The  $\text{O}_2$  cycle of the ocean is strongly impacted by climate change through physical and biogeochemical mechanisms illustrated in **Figure 4a** and related through Equation 1. Dissolved gases are less soluble in warmer waters, reducing the concentration of  $\text{O}_2$  at saturation ( $\text{O}_2^{\text{sat}}$ ). At the

surface, this has little impact on  $p\text{O}_2$ , which rapid gas exchange maintains near equilibrium with the atmosphere. However, the nonlinearity of  $K_{\text{H}}(T)$  means that a warmer surface ocean will result in lower interior  $p\text{O}_2$  even if the total concentration of  $\text{O}_2$  consumed by respiration (i.e.,  $R_{\text{w}}/\Psi_{\text{w}}$ , or AOU) does not change. Thus, the impact of warming alone, combined with surface equilibration, reduces  $p\text{O}_2$  in deep water. This effect is typically small, however, compared with changes that arise from changes in either respiration rate ( $R_{\text{w}}$ ) or ocean circulation rate ( $\Psi_{\text{w}}$ ), a combination of which is implied by historical observations and simulations in Earth system models (Figure 4b–d; see below).

Historical observations show that over the past several decades, as the ocean has absorbed heat from anthropogenic climate warming, it has also lost  $\sim 2\%$  of its  $\text{O}_2$  inventory (Ito et al. 2017, Schmidtke et al. 2017). The loss of  $\text{O}_2$  exhibits a strong correlation with temperature, and the slope increases systematically with depth, consistent with theoretical vectors in Figure 4a. At the surface, the  $\Delta\text{O}_2/\Delta T$  slope follows that of solubility [ $K_{\text{H}}(T)$ ], yielding no appreciable change in  $p\text{O}_2$ , but steepens with depth, exceeding what can be accounted for by solubility alone (Figure 4c). The increase in global  $\text{O}_2$  decline in deeper waters implies that the  $\text{O}_2$  demand/supply ratio in the interior of the ocean has also increased, leading to lower  $p\text{O}_2$  of the subsurface waters as temperatures have risen. The  $\text{O}_2$  trend and the slope of the  $\text{O}_2/T$  relationship in historical observations also vary strongly among ocean regions (Ito et al. 2019, Stramma et al. 2012). Thus, the loss of  $\text{O}_2$  per degree of warming historically experienced by marine populations has likely varied significantly according to the range of ocean depths, as well as the regions, in which they live.

The loss of  $\text{O}_2$  on a global scale has become detectable in observations, but both the attribution of underlying causes and the projection to future (and past) climate states rely heavily on Earth system models, which parameterize the mixing, production, and consumption of  $\text{O}_2$  (Figure 4b–d; see Supplemental Appendix C). Such models successfully reproduce the qualitative global distribution of  $\text{O}_2$  and aspects of its historical variability but also exhibit systematic regional and temporal biases, especially in low- $\text{O}_2$  regions (Shepherd et al. 2017). The apparent tendency of ESMs to underestimate the magnitude of historical  $\text{O}_2$  variability (Long et al. 2019, Oschlies et al. 2018) leaves substantial uncertainty about future projections.

Earth system models uniformly project declining global rates of both  $\text{O}_2$  supply and demand, though both exhibit strong regional variability. Reduced rates of ventilation of the ocean interior are due to increased density stratification from surface warming and freshening. At a global scale, net primary productivity in the surface ocean also declines, especially in the low latitudes, where it becomes even more strongly nutrient limited (Kwiatkowski et al. 2020). Reduced nutrient supply is driven by a combination of weaker trade winds and equatorial upwelling (Terada et al. 2019) and nutrient depletion from source waters originating at high latitudes (Fu et al. 2018, Marinov et al. 2006). The slower production of organic matter at the surface reduces the particle flux to the deep ocean, causing a global decline in the rates of microbial respiration that account for most of the deep  $\text{O}_2$  undersaturation. On a global basis, the reduction of circulatory supply ( $\Psi_{\text{w}}$ ) exceeds the reduction in respiratory demand ( $R_{\text{w}}$ ), leading to a decline in  $\text{O}_2$  and a lower global mean  $p\text{O}_2$ .

A common prediction of state-of-the-art Earth system models is that in the tropical OMZ,  $\text{O}_2$  remains relatively stable or even increases in a warming climate (Figure 4b). The tropical immunity from deoxygenation stems from the decline in microbial  $\text{O}_2$  consumption (i.e.,  $R_{\text{w}}$ ) discussed above. The cumulative effect of slower  $\text{O}_2$  consumption grows along the circulation path to reach a maximum in the tropical thermocline, where it becomes comparable to—and thus largely cancels out—the effect of lower gas solubility. The compensation between  $\text{O}_2$  supply and demand in the tropical thermocline is found in modern and past climate warmings (Fu et al. 2018, Ilyina & Heinze 2019, Matear & Hirst 2003, Penn et al. 2018), likely due to fundamental coupling of nutrient and  $\text{O}_2$  cycles. In a nutrient-limited ocean, a reduced circulatory  $\text{O}_2$  flux to the deep sea

## Supplemental Material >

is inherently coupled to microbial demand, as the same physical circulation supplies the nutrients to fuel surface primary producers.

The combination of these mechanisms leads to opposing  $pO_2$  trends in the tropics and the higher latitudes (**Figure 4c,d**). In the high latitudes, the additional  $O_2$  consumption due to a more complete surface nutrient drawdown ensures that  $pO_2$  declines significantly beyond the solubility effect. In contrast, the tropical compensation between  $O_2^{sat}$  and AOU yields a small net change in  $O_2$ , and across models, the sign of the trend is not robust. However, reconstructed changes in the world's largest suboxic zone, in the Pacific Ocean, reveal a close coupling to tropical trade winds, which are robustly predicted to weaken as the climate warms such that future suboxic zones should shrink even while global  $O_2$  declines (Deutsch et al. 2014), a tendency confirmed by recent analyses of Earth system models (Busecke et al. 2022). More importantly, in all models, even those projecting a slight tropical  $O_2$  decline, the driving force for biological uptake— $pO_2$ —eventually rises (**Figure 4d**).

The net effect of these ocean dynamics is a redistribution of  $pO_2$  from the  $O_2$ -rich higher latitudes toward the low- $O_2$  tropics, and this has significant consequences for marine life. The reduction of anoxia in the tropics, even while oxygen is steadily declining globally, suggests that the habitat of anaerobic microbes could contract, weakening water-column nutrient removal. At the same time, the OMZ barrier to vertical migration by tropical marine animals (Bianchi et al. 2013) would weaken, with potential to partially counteract the impact of higher temperatures on organismal demand. We return to these consequences in Section 3.

## 2.2. $O_2$ Supply and Demand at the Organism Scale

At an organismal scale, the balance of  $O_2$  supply and demand (Equation 2) is also strongly governed by temperature (**Figure 5**). The impact of temperature on both metabolic rates of  $O_2$  demand and the biophysical  $O_2$  supply needed to fuel them has long been a focus of marine biology and thermal physiology (see **Supplemental Appendix D**). Classic experiments on goldfish by Fry & Hart (1948) illustrate many of the salient organismal responses to temperature and  $O_2$  (**Figure 5a**).

For an animal at rest, its rate of  $O_2$  consumption can be measured as the  $O_2$  depletion rate in a closed and well-mixed tank (**Figure 5a**). For most organisms, the rate initially remains constant as  $O_2$  drops, because metabolism is not limited by  $O_2$  availability. As ambient  $O_2$  continues to fall, a  $pO_2$  threshold is eventually reached below which the metabolic rate must slow in proportion to the declining ambient  $O_2$ . At a given temperature, these two distinct phases define the  $O_2$  demand and the  $O_2$  supply, respectively (**Figure 5a**). The balance between supply and demand, which lies at the intersection of these lines, occurs at a critical oxygen threshold, defined as  $pO_2^{crit}$  (see Equation 2). For  $pO_2 < pO_2^{crit}$ , resting demand cannot be met and must be suppressed. For  $pO_2 > pO_2^{crit}$ , the ambient  $pO_2$  has the potential to supply more than is needed for resting demand, allowing for energetic expenditure to rise beyond minimal resting or maintenance levels. We refer to  $pO_2^{crit}$  at a reference temperature as resting hypoxia vulnerability and to its inverse as resting hypoxia tolerance ( $A_o$ , 1/atm).

An increase in  $pO_2^{crit}$  with temperature within species is among the most pervasive patterns across diverse marine taxa (**Figure 5b**). It arises from the thermal acceleration of metabolic rates, a trend also seen in lethal  $O_2$  concentration thresholds (**Figure 2b**). The increase of  $pO_2^{crit}$  with temperature leads to a simple but robust projection: that ocean warming alone will pose a serious challenge for any marine species that already experiences  $O_2$  limitation in its natural habitat. The severity will be greater still if that habitat also undergoes a drop in  $pO_2$ , as expected for most of the ocean (**Figure 4b**). That is, marine organisms are confronted with a dual challenge: an increased ratio of  $O_2$  demand relative to biophysical supply and an ocean that presents them with less  $O_2$  due to an analogous imbalance at the global scale.

---

**Hypoxia tolerance:** in the resting state, the inverse of  $pO_2^{crit}$  at a reference temperature and body mass; in the active state, the resting value divided by the ratio of sustained to resting metabolic rate

---

**Supplemental Material** >

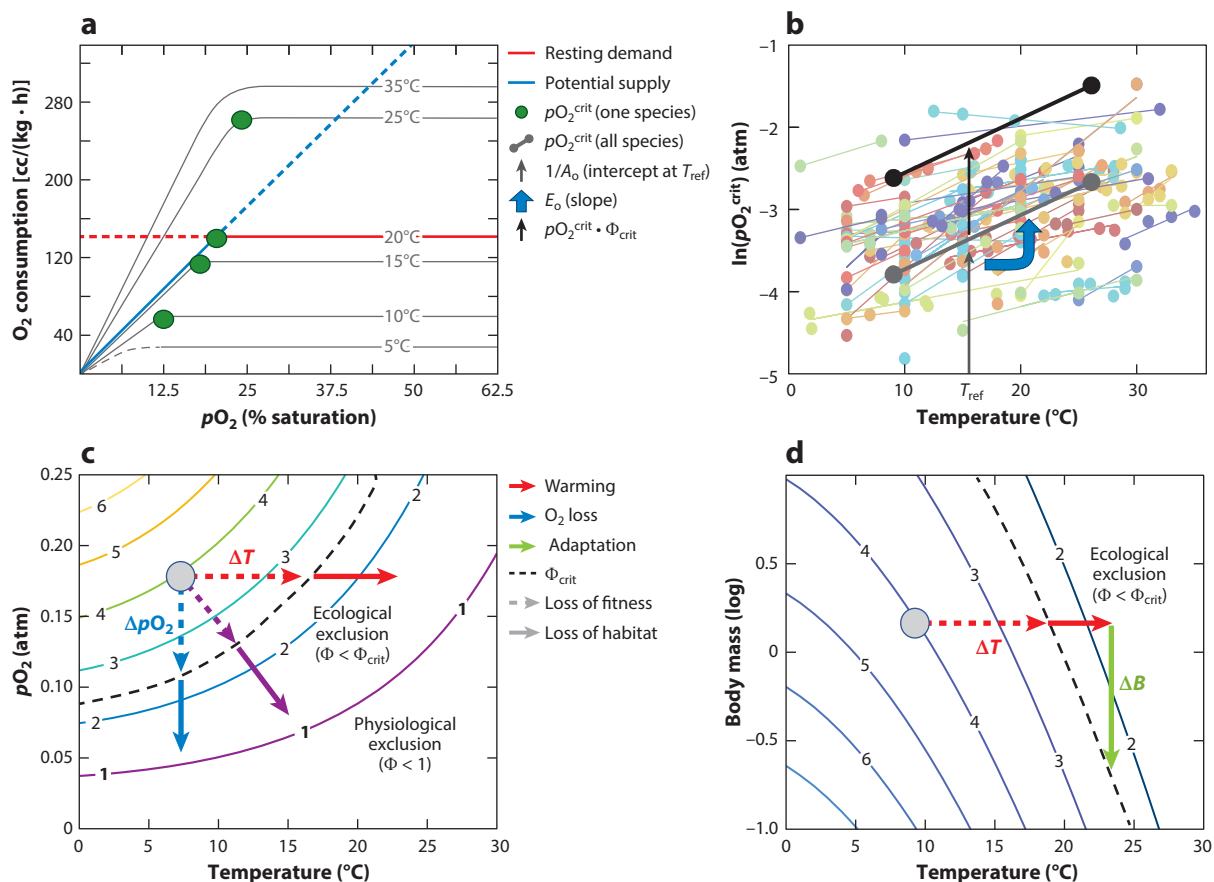


**Figure 5**

Relationship between temperature and  $O_2$  supply and demand in marine organisms. (a) Rates of resting metabolic  $O_2$  demand (horizontal line heights) increase with temperature faster than potential organismal  $O_2$  supplies (slanted line slopes), causing their intersection, the critical  $O_2$  threshold ( $pO_2^{crit}$ ; green circles), to increase with temperature in laboratory experiments. Line portions based on Fry & Hart's (1948) experimental data are extended with dashed lines to illustrate where the observed rates become potential rates that are not realized because either supply is not adequate to fuel demand (dashed red line) or resting demand is too low to use the full supply capacity (dashed blue line). (b)  $pO_2^{crit}$  measurements versus temperature show wide interspecies variation (colored points) and can be used to calculate two key species traits, resting hypoxia tolerance ( $A_o$ ) and its temperature sensitivity ( $E_o$ ). (c,d) A model of temperature and body size-dependent organismal  $O_2$  supply/demand rates, termed the metabolic index, characterizes the environment's capacity to sustain aerobic metabolism ( $\Phi$ ; Equation 3). For a typical species in which metabolic rate increases with temperature faster than  $O_2$  supply (i.e.,  $E_o > 0$ ) (panel c), ocean warming and/or  $O_2$  loss depletes  $\Phi$ , leading to a reduction in organism activity (fitness) until an energetic threshold for population sustenance ( $\Phi_{crit}$ ) is reached, below which aerobic habitat is lost and the species is extirpated. If  $\Phi$  is depleted below 1, even resting metabolism cannot be maintained. If rates of metabolism increase with body size more strongly than does  $O_2$  supply (i.e.,  $\varepsilon < 0$ ) (panel d), a reduction of  $\Phi$  can be potentially ameliorated by ceasing growth at smaller body size until an anatomically or ecologically viable size limit is reached. Abbreviation:  $pO_2$ ,  $O_2$  partial pressure. Panel a adapted with permission from Fry & Hart (1948); panel b adapted from Deutsch et al. (2020).

Projecting the biological impact of climatic changes in temperature and  $pO_2$  requires a model for the balance of  $O_2$  supply and demand of aquatic breathers, applicable across a wide range of species and ocean regions. While Earth system models represent the numerous factors driving variation in oceanic  $O_2$  demand ( $R_w$ ) and supply ( $\Psi_w$ ) through complex spatially resolved and time-dependent equations too numerous to list (but see **Supplemental Appendix C**), models

of analogous organismal rates typically rely on simple empirical scaling relationships (Schmidt-Nielsen 1984). These relationships allow Equation 2 to represent, explicitly but approximately, the dependence of physiological rates of O<sub>2</sub> demand ( $R_o$ ) and supply ( $\Psi_o$ ) on environmental conditions, such as temperature and  $pO_2$ , and species traits, including body mass.

Resting metabolic rates are well described by an exponential dependence on temperature and power law dependence on body mass ( $B$ ):  $R_o = \alpha_D B^\delta \text{Ar}(E_d, T)$ , where  $\alpha_D$  is the rate at a reference temperature and body size and Ar is the Arrhenius equation (Gillooly et al. 2001) (Table 1). The allometric and thermal sensitivities ( $\delta$  and  $E_d$ , respectively) are positive when the rate rises with body size or temperature. The three parameters ( $\alpha_D$ ,  $\delta$ , and  $E_d$ ) are traits that characterize the metabolism of a species. A similar scaling can be applied to the potential rate of O<sub>2</sub> supply:  $\Psi_o = \alpha_S \cdot B^\sigma \cdot \text{Ar}(E_s, T)$ , where  $\alpha_S$  is the rate coefficient per unit  $pO_2$  at a reference temperature and body mass, and  $E_s$  and  $\sigma$  are the respective sensitivities (Deutsch et al. 2020).

The ratio of rates of potential O<sub>2</sub> supply to resting demand defines the metabolic index ( $\Phi$ ) (unitless):

$$\Phi = A_o \cdot pO_2 \cdot B^\varepsilon \cdot \text{Ar}(-E_o, T) = pO_2 / pO_2^{\text{crit}}, \quad 3.$$

where  $A_o$  is the ratio of O<sub>2</sub> supply coefficient to demand rate at the reference temperature and body mass, equivalent to resting hypoxia tolerance;  $E_o$  is the organism's thermal sensitivity; and  $\varepsilon$  is its body size scaling. The value of  $A_o$  determines the response of  $\Phi$  to changes in  $pO_2$ , whereas  $E_o$  quantifies the response of  $\Phi$  to warming (or cooling) absent a change in  $pO_2$  and  $\varepsilon$  encapsulates the response to a change in body mass. All three traits are defined by the net effect of both supply and demand traits (i.e.,  $A_o = \alpha_S / \alpha_D$ ,  $E_o = E_d - E_s$ , and  $\varepsilon = \sigma - \delta$ ).

The metabolic index measures any environment's capacity to sustain energy demand beyond the minimum maintenance level, for any species with known traits. It represents the potential energy available for growth and ecological activity and the upper limit on the ratio of maximum to minimum rates of metabolism, a quantity commonly realized in laboratory experiments as aerobic scope (Brett 1971, Chabot et al. 2016). By construction,  $\Phi$  can also be expressed as the ratio of oceanic  $pO_2$  to the critical value for an organism at rest,  $pO_2^{\text{crit}}$ , thus combining the oceanographic expression of O<sub>2</sub> balance (Equation 1) with the physiological threshold at the organismal scale (Equation 2).

Traits derived from experimental respirometry reveal wide variation across diverse species (Figure 5b). For most species, hypoxia tolerance rises less with temperature (mean  $E_o \sim 0.4$  eV) than would be expected from metabolism alone (mean  $E_d \sim 0.7$  eV) (Deutsch et al. 2020). This is because temperature elevates not only metabolic demand but also the efficacy of the O<sub>2</sub> supply chain (i.e.,  $\Psi_o$ ), seen in the higher slope of the O<sub>2</sub>-limited portion of the respirometry curves in warmer water (Figure 5a). As anticipated by Equation 2, the impact of a rise in  $R_o$  on  $pO_2^{\text{crit}}$  can be partially offset by a concomitant increase in  $\Psi_o$ , thus making hypoxia tolerance less temperature sensitive for species that can accelerate their O<sub>2</sub> supply (i.e.,  $E_s > 0$ ) to partially compensate for a faster metabolic rate (i.e., because  $E_o = E_d - E_s$ ).

Growth in body size may also alter an organism's potential O<sub>2</sub> supply/demand ratio. Ontogenetic changes in hypoxia tolerance can be assessed by measuring  $pO_2^{\text{crit}}$  across a range of body sizes within a species (Pan et al. 2016). Such experiments are rare compared with those conducted across a temperature range, but they yield analogous patterns. The allometric exponent ( $\varepsilon$ ) also exhibits high interspecific variability with strong polarity: Trait values skew strongly negative ( $\varepsilon < 0$ ), indicating that smaller is better for most sampled species. In contrast to thermal sensitivity, the allometric dependence itself increases with body size across the tree of life, from single cells ( $\varepsilon \ll 0$ ) to macrofauna ( $\varepsilon \sim 0$ ), due to convergence of its constituent scalings for O<sub>2</sub> supply and demand (i.e., because  $\varepsilon = \sigma - \delta$ ) (Deutsch et al. 2022). Consistent with  $\varepsilon \sim 0$  for large body

#### Metabolic index ( $\Phi$ ):

the ratio of temperature-dependent rates of O<sub>2</sub> supply to demand, which depends on environmental temperature and  $pO_2$  as well as the species' traits, including temperature and allometric sensitivity

**Aerobic scope:** the difference between an organism's measured maximum and minimum metabolic rates, considered an experimental measure of the energy potentially available for growth and activity



sizes, the well-studied allometric scaling of intraspecific  $O_2$  demand among marine fish (Clarke & Johnston 1999) is closely matched to the body size dependence of  $O_2$  exchange surfaces (Gillooly et al. 2016, Pauly 2021). Allometric scaling of  $O_2$  supply and demand diverge at smaller body sizes, where  $O_2$  supply is governed by diffusive boundary layers at the body surface (Deutsch et al. 2022).

The aerobic balance of any organism can be altered by changes in temperature or  $pO_2$  or growth in body size, and these time-dependent balances can be computed using the metabolic index, by combining species traits with measured environmental conditions (**Figure 5c,d**). As  $pO_2$  decreases,  $\Phi$  declines for all species, although the absolute change depends on  $A_o$ . In contrast,  $\Phi$  can decrease with temperature for species in which metabolic rate increases faster than  $O_2$  supply ( $E_o > 0$ ; colder is better) or increase under the opposite scenario ( $E_o < 0$ ; warmer is better), which is relatively rare across sampled biota (but see below). As the magnitude of  $\Phi$  declines, the aerobic energy that can be supplied by the available  $O_2$  declines, and the species loses part of the energy available for growth or activity. The loss of potential aerobic scope can be driven by either warming or loss of  $O_2$ , and its magnitude will depend on both species traits and the rates of environmental change. For organisms whose metabolic rate increases with body size by a greater factor than its  $O_2$  supply capacity does (i.e.,  $\varepsilon < 0$ ), any decrease in  $O_2$  supply/demand ratio (i.e.,  $\Phi$ ) may be partially counteracted by limiting growth (**Figure 5d**). If the decline of  $\Phi$ , accounting for body size and other adaptations, exceeds the threshold of energy required to maintain an ecologically viable population, termed  $\Phi_{crit}$ , the species will experience a loss of aerobic habitability and become locally extirpated.

The metabolic index can be derived from dynamical models that directly simulate the time-dependent metabolism of aquatic organisms, allowing several important generalizations, including more complex temperature dependencies and sensitivities to other environmental conditions (Endress et al. 2022). For example, a generalized metabolic index can reproduce hypoxia tolerances that exhibit a thermal optimum (Boag et al. 2018, Duncan et al. 2020), as opposed to a simple exponential temperature dependence. Such situations arise when multiple steps in the  $O_2$  supply chain have distinct temperature sensitivities. For example, biophysical pumping of  $O_2$  in the circulatory system often increases with temperature faster than metabolic rate but ceases to be an effective strategy for increasing  $O_2$  supply when diffusion, which is very weakly temperature dependent, becomes more limiting. Thus, a switch in  $O_2$  supply limitation from biophysical mechanisms with high  $E_s$  to diffusion with low  $E_s$  can cause the effective  $E_o$  to change sign across the temperature range, such that  $pO_2^{crit}$  attains a thermal optimum (Endress et al. 2022).

Finally, while the formulation in Equation 3 is written to highlight the temperature sensitivity of aerobic energy balance, it is easily generalized to represent the effect of other biotic stressors. For example, ocean acidification may impose an energetic cost or alter the efficacy of  $O_2$  supply. While currently available data suggest that these impacts are relatively small (Birk et al. 2018, Ern et al. 2016), they can be readily included in the functional dependence of  $\alpha_D$  and  $\alpha_S$  in cases where physiological data reveal significant unresolved environmental effects.

### 3. BIOGEOGRAPHY, BIODIVERSITY, AND BIOGEOCHEMISTRY

If temperature-dependent tolerance to hypoxia constrains the fitness of marine species in the natural environment, then species geographic range limits should align with hydrographic conditions that reflect  $O_2$  limitation of active metabolism. A growing number of studies are documenting close correspondence among species geographic ranges over space and time, as well as aerobic habitat barriers governed by metabolic index traits (Burford et al. 2022; Clarke et al. 2021; Deutsch et al. 2015, 2020; Duncan et al. 2020; Franco et al. 2022; Howard et al. 2020; Lucey et al. 2023).

Evaluating the role of temperature-dependent hypoxia in restricting species geographic ranges requires the integration of several distinct observational datasets, including laboratory

respirometry experiments to estimate metabolic index traits (**Figure 5b**), climatological or time-dependent hydrographic measurements of temperature and  $O_2$  (e.g., **Figure 2a**), and spatial distributions of species occurrences. In most species for which all such data are available, range boundaries are more strongly aligned with a constant metabolic index than with either temperature or  $pO_2$  alone (Deutsch et al. 2020). The correspondence between  $\Phi$  and range limits can be observed geographically in cases where species are well sampled, for example, in Atlantic cod (*Gadus morhua*), where equatorial range limits on both sides of the basin coincide with a similar lower limit of  $\Phi$ , above which the species is widely distributed and below which it is rare (**Figure 6a**).

Variations in metabolic index traits give rise to distinct geographic habitat niches (Deutsch et al. 2020). For species with large temperature sensitivities ( $E_o$ ),  $\Phi$  declines strongly from cool to warm water, limiting species to high latitudes, whereas species with weak or negative  $E_o$  can persist in the warm surface waters of the tropics but are excluded at depth by OMZs. For a given  $E_o$ , a species active hypoxia tolerance ( $A_c = A_o/\Phi_{crit}$ ) also modulates the patterns of viable habitat, with high  $A_c$  conferring the ability to inhabit the lowest- $O_2$  waters of tropical OMZs (Wishner et al. 2018) and low  $A_c$  restricting habitat to high- $pO_2$ , low-temperature extratropical surface waters.

The alignment of species range boundaries with temperature-dependent hypoxia limits becomes more visible by converting species geographic distributions to the observed temperature and  $pO_2$  niches that they inhabit (**Figure 6b**). The observed temperature dependence of lower  $pO_2$  boundaries often reflects the underlying physiological sensitivities of the organismal  $O_2$  balance measured in direct respirometry experiments (i.e.,  $pO_2^{crit}$ ). However, the lowest inhabited values of  $pO_2$  in the environment exceed experimental thresholds in the laboratory by the factor  $\Phi_{crit}$  that represents the additional energy required for ecological activity, including growth, reproduction, mobility, and feeding. Such state-space habitat diagrams demonstrate that habitat-bounding conditions of temperature or  $pO_2$  are the product of intrinsic physiological tolerances ( $pO_2^{crit}$ ) elevated by ecological energy requirements ( $\Phi_{crit}$ ). Biogeographic assessments of  $\Phi_{crit}$  are consistent with laboratory estimates of sustained metabolic rates in marine species (Killen et al. 2016) and with field-based estimates of terrestrial taxa (Hammond & Diamond 1997). This correspondence supports the notion that aerobic habitat barriers for sustained ecological activity limit the geographic ranges of marine species, even in regions outside of traditional OMZs.

If the geographic ranges of marine species are commonly limited by temperature-dependent hypoxia tolerance traits, then the frequency distribution of those traits should also be able to predict key patterns of marine biodiversity. The richness of marine species varies strongly with latitude, more than doubling from the poles to the tropics (**Figure 6c**). A similar latitude diversity gradient is seen across many taxa in both marine and terrestrial ecosystems. However, the ocean's gradient is bimodal, exhibiting an equatorial dip in biodiversity that interrupts the broader tropical richness maximum (Chaudhary et al. 2021, Tittensor et al. 2010), a feature that arose since the last ice age (Yasuhara et al. 2020). This dip in species richness in warm equatorial waters provides a unique signal for testing mechanisms that could limit the diversity of species in the tropical ocean but would not operate on land.

Analyses of species richness patterns have commonly highlighted strong correlations with sea surface temperature (Tittensor et al. 2010). Recent comparisons of ocean temperatures with measured physiological limits of marine species demonstrated that even peak diurnal surface temperatures rarely exceed critical thermal maxima (Deutsch et al. 2020, Pinsky et al. 2019). Indeed, upper thermal limits alone do not predict the equatorial dip in species richness (**Figure 6c**). Short-term assays may overestimate thermal tolerance, as thermal tolerance on ecologically relevant timescales declines to levels comparable with ocean temperatures (Molina et al. 2023).

The low  $O_2$  of the tropical subsurface waters (**Figure 2a**) provides a compelling explanation for the reduced equatorial richness, especially in conjunction with the warm temperatures there that

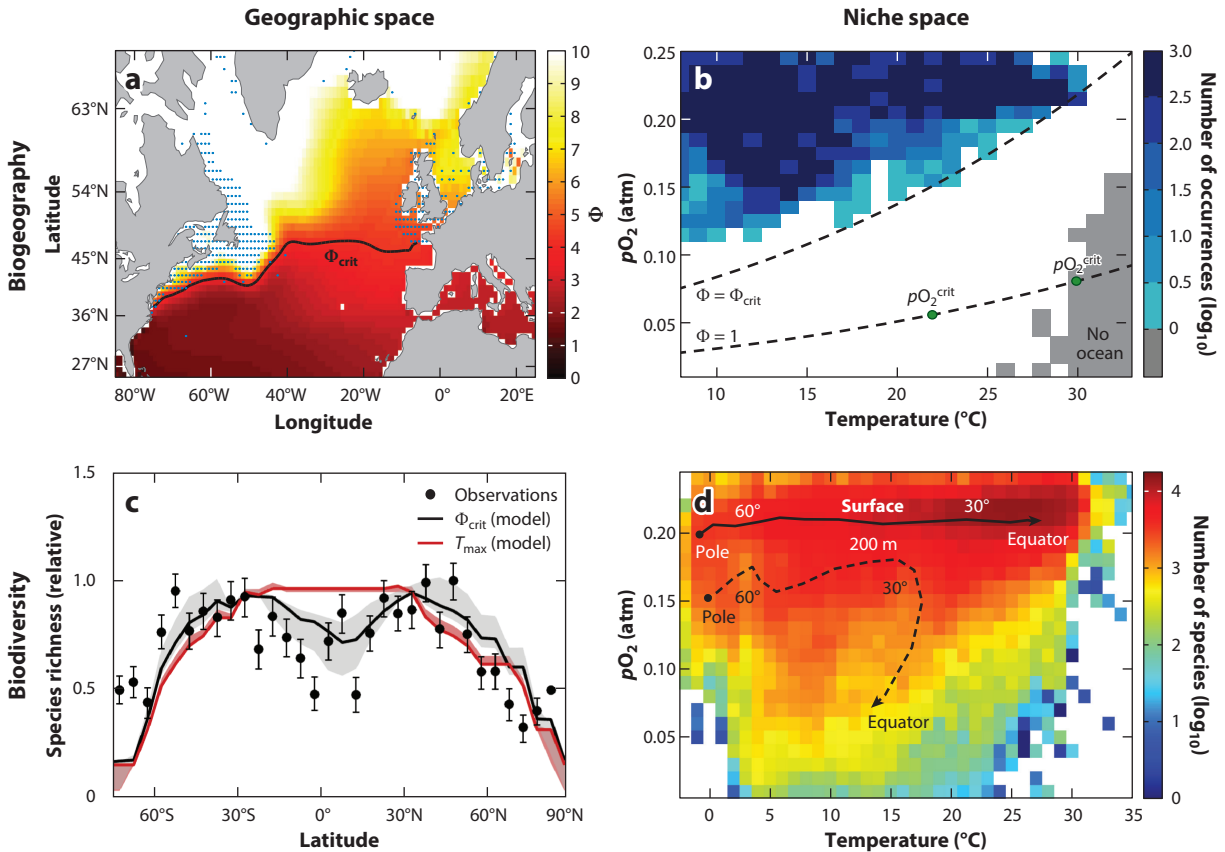


**Figure 6**

How climate and species traits shape patterns of biogeography and biodiversity in geographic and niche space. (*a,b*) Species range limits in geographic space and inhabited temperature– $pO_2$  niche space align with minimum thresholds of  $\Phi$  required to sustain an ecologically viable population ( $\Phi_{crit}$ ). As shown in panel *a*, the intrabasin equatorial range boundary of Atlantic cod (*Gadus morhua*) coincides with a lower value of  $\Phi$  mapped from observed hydrographic conditions (temperature and  $pO_2$ ) and traits ( $A_o$  and  $E_o$ ) that are derived from  $pO_2^{crit}$  measurements. Panel *b* shows that the inhabited lower  $pO_2$  levels of summer flounder (*Paralichthys dentatus*), a fish from the western Atlantic, increase with temperature, consistent with a mechanism of temperature-dependent hypoxia tolerance implied by respirometry measurements of  $pO_2^{crit}$  (green circles). The elevation of the lowest inhabited ocean  $pO_2$  levels above laboratory  $pO_2^{crit}$  measures the additional energy required for growth and ecological activity above the resting metabolic demand (i.e.,  $\Phi_{crit}$ ). (*c*) Observed species richness displays a bimodal gradient versus latitude, which can be reproduced by a trait-based aerobic habitat model, the metabolic index ( $\Phi$ ), including species' lower temperature limits, applied to observed three-dimensional distributions of temperature and  $O_2$ . By contrast, if warm-edge habitat limitation is modeled based on species' observed upper thermal limits ( $T_{max}$ ) (i.e., not accounting for  $O_2$ , as is done with  $\Phi$ ), model richness shows a broad peak across the equator. (*d*) Observed species richness mapped into inhabited temperature– $pO_2$  niche space shows that richness declines with  $pO_2$  and displays a unimodal relationship with temperature in subsaturated waters. Lines show the average ocean temperature– $pO_2$  relationship along the global pole-to-equator gradient at the surface (solid arrow) and at 200 m (dashed arrow). Abbreviation:  $pO_2$ ,  $O_2$  partial pressure. Panel *a* adapted from Deutsch et al. (2015); panel *b* adapted from Deutsch et al. (2020); panel *c* adapted with permission from Penn & Deutsch (2022), where  $\Phi$  model details are provided. The  $T_{max}$  curve in panel *c* follows the same methods but replaces warm-edge habitat limitation by  $\Phi$  with species' upper temperature thresholds using observations from Pinsky et al. (2019). Modeled species richness is summed from the ocean surface to a maximum depth (500-m lines, 50- and 5,000-m shading). The richness observations (black circles) are from Chaudhary et al. (2017) and are based on a global dataset of species occurrences (the Ocean Biodiversity Information System; <https://obis.org>), which was paired with climatological hydrographic conditions (Boyer et al. 2018) to generate the niche-space richness in panel *d*.

elevate most species'  $pO_2^{\text{crit}}$ . An aerobic limit on equatorial species richness has recently been supported by global simulations of biogeographic patterns across thousands of model species (Penn & Deutsch 2022). To predict species' three-dimensional distributions of aerobic habitat, global observations of ocean temperature and  $O_2$  were combined with the observed frequencies of species traits describing the temperature-dependent hypoxia limits (e.g., **Figure 5b**). The model predictions demonstrate that tropical aerobic conditions (high temperature and low  $pO_2$ ) combined with the tolerance traits of modern species drive  $\Phi$  below its ecological limit ( $\Phi_{\text{crit}}$ ) for many taxa, resulting in fewer species being able to inhabit the equator than can inhabit subtropical latitudes.

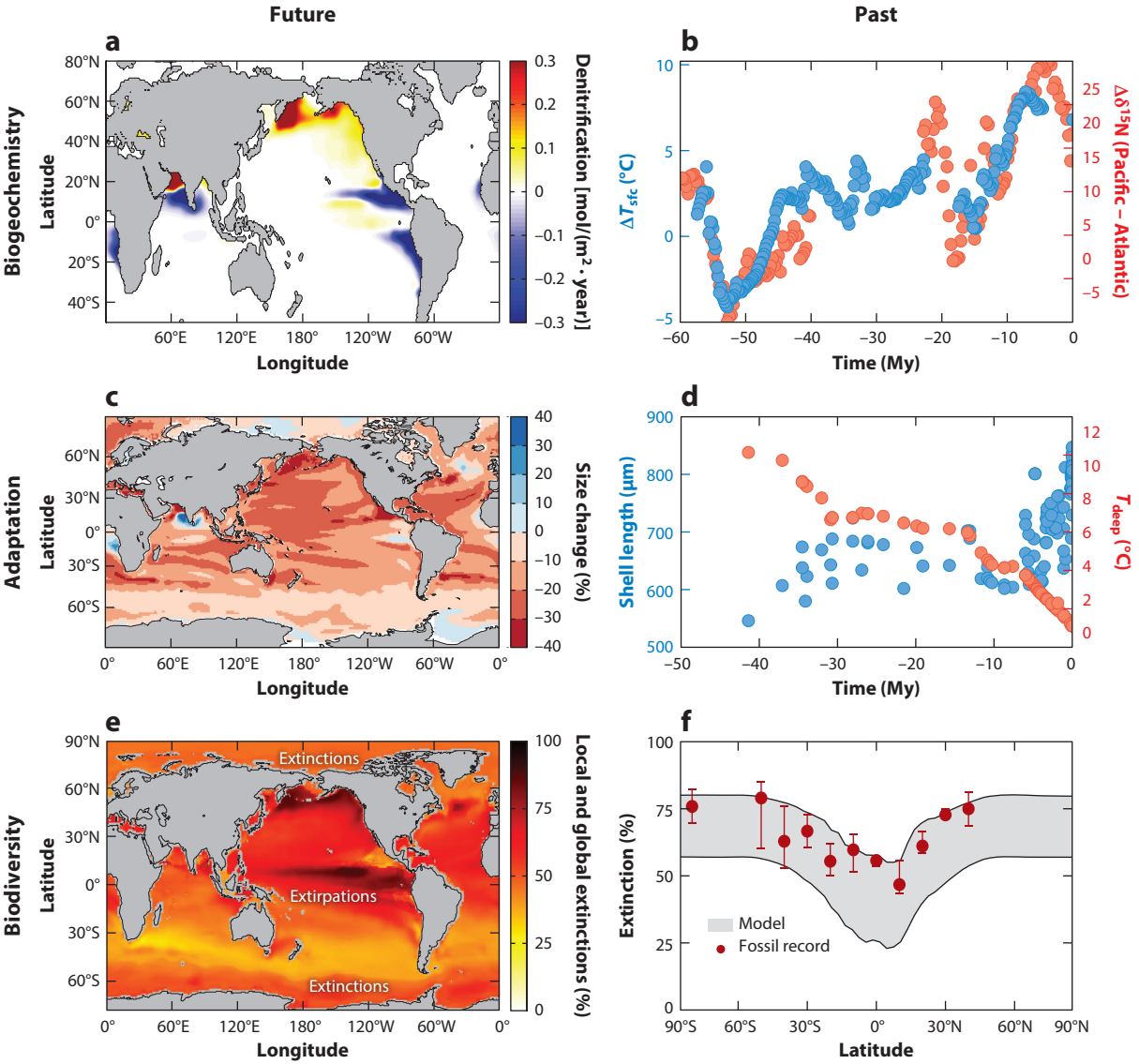
A prominent role for  $O_2$  in biodiversity patterns is also supported by observations of species richness viewed against temperature– $pO_2$  niche space, where richness strongly declines with  $pO_2$  at all temperatures (**Figure 6d**). At the surface, where  $pO_2$  is near saturation, richness increases with temperature (latitude) but shows a unimodal pattern versus temperature in undersaturated water, with a temperature of peak richness that increases with  $pO_2$ . This pattern implies that at higher  $pO_2$ , more species can persist in warmer waters, consistent with species temperature-dependent  $pO_2^{\text{crit}}$  measurements (e.g., **Figures 5b** and **6b**). These observations extend the findings from regional correlations of  $O_2$  and diversity (Sperling et al. 2016) across the full oceanic range of  $O_2$  and temperature.

Anthropogenic climate change will alter the aerobic constraints that naturally limit the habitat of marine animals and microbes. Projections of climate change from Earth system models can be combined with models of species responses to derive estimates of impending shifts in large-scale patterns of biogeochemistry, physiological adaptation, and biodiversity. We highlight projections for key biological responses that have been tested against paleoclimate evidence (**Figure 7**).

Some of the largest and most surprising impacts of climate warming on marine ecosystems are projected in regions with the lowest  $O_2$  (**Figure 7a,b**). If the tropical ocean becomes better oxygenated, anoxic zones could shrink, contrary to the widely anticipated expansion seen in recent decades. Indeed, model simulations of the  $O_2$  response to climate in this century imply that denitrification may be strongly reduced in the tropics, although regions of more intense anaerobic nitrogen loss may expand in higher-latitude regions (Bianchi et al. 2018), particularly the North Pacific (**Figure 7a**), where  $O_2$  is already low enough to support anaerobic metabolism in sediments and large particles (**Figure 2a**). This shift is driven by the tendency of models to oxygenate the tropics at the expense of high latitudes. Because near-anoxic conditions are confined to small water volumes at the tail of the volumetric distribution (**Figure 2b**), anoxic and suboxic ( $O_2 < 5 \mu\text{M}$ ) waters are intrinsically sensitive to small variations in  $O_2$  concentration (Deutsch et al. 2011), similar to the impact of climate warming on atmospheric heatwaves.

Paleoceanographic observations support global Earth system model projections of a weaker tropical nitrogen loss in the future due to climate warming. The removal of bioavailable  $\text{NO}_3^-$  by anaerobic (denitrifying) bacteria elevates the isotope ratio ( $\delta^{15}\text{N}$ ) of the local  $\text{NO}_3^-$  reservoir, a signal that is transported to the photic zone, taken up by phytoplankton, and exported in organic matter to underlying sediments. Over most of the twentieth century, sedimentary  $\delta^{15}\text{N}$  declined near the world's largest anoxic zone, in the eastern tropical North Pacific. On a century timescale, slower nitrogen removal is linked to weakening of the wind-driven equatorial upwelling (Deutsch et al. 2014), a trend that is characteristic of future warming scenarios (IPCC 2021). A reduced nitrogen loss in warmer climates is also inferred from sediment records spanning millions of years (Auderset et al. 2022), in which the large  $\delta^{15}\text{N}$  difference between ocean basins with anoxic zones (the Indo-Pacific) versus those without (the Atlantic) collapses during warm climate intervals (**Figure 7b**). On such long timescales, extratropical mechanisms, including the nutrient status of high latitudes found in multicentury simulations, are also likely to become important.

A warming-driven contraction of anoxic zones and associated reduction of anaerobic microbial nitrogen losses appears increasingly consistent with both recent model projections and paleo observations (Figure 7*a,b*). However, a robust quantitative assessment is impeded by several factors. The current size and structure of anoxic zones are only crudely delineated by observations and simulated by Earth system models, whose forecasts are dependent on highly parameterized mixing processes (Ito et al. 2022). The rates of microbial nitrogen cycling in these zones are also sensitive to numerous factors missing or coarsely represented in Earth system models, including microbial community structure (Penn et al. 2016), variations in organic matter stoichiometry (Babbin et al. 2014, DeVries & Deutsch 2014), and the physical and biogeochemical dynamics of particles (Cram et al. 2018). A robust quantitative evaluation of anoxic zone changes and the broader



(Caption appears on following page)



**Figure 7** (Figure appears on preceding page)

Climate change impacts on biogeochemistry (ocean nitrogen cycling), adaptation (animal body size), and biodiversity (extinction risk) projected using Earth system models that simulate future climate warming and ocean O<sub>2</sub> loss (panels *a*, *c*, and *e*) and reconstructed from paleo records and paleo simulations (panels *b*, *d*, and *f*). (*a*) Change in water-column nitrogen removal by anaerobic microbes forced by future O<sub>2</sub> changes (see **Figure 4b**). (*b*) Geochemical proxies for anoxia and climate over the past 60 My. Nitrogen isotopes from Pacific and Atlantic sediment cores show a declining gradient (red circles, right y axis) during intervals of weaker latitudinal temperature gradient (blue circles, left y axis), indicating a reduction in the rate of fractionating nitrogen loss in Pacific anoxic zones during warmer climates (Auderset et al. 2022). (*c*) Change in organism body size required to counteract this century's projected decline in upper-ocean O<sub>2</sub> supply/demand ratios ( $\Phi$ ) for species at the base of the food web. (*d*) Sizes of deep-sea ostracod shells (blue circles, left y axis) and deep-ocean temperatures (red circles, right y axis) since the Eocene (Hunt & Roy 2006). Cooling abyssal waters are strongly correlated with increasing ostracod body size, consistent with metabolic expectations (**Figure 5**). (*e*) Projected extirpations and extinctions of marine animals due to anthropogenic climate warming and oceanic O<sub>2</sub> loss by 2300 CE in the RCP8.5/SSP5 emissions scenarios. Extirpations are greatest for species inhabiting lower latitudes, but high-latitude species are most vulnerable to global extinction. (*f*) Extinction versus latitude in paleoclimate simulations of the end-Permian and observed from the fossil record. In panels *a*, *c*, and *e*, the Earth system models are forced by a high-greenhouse-gas-emissions scenario (see inset in **Figure 10** later in this article) for the end of the century (panels *a* and *c*) and to 2300 CE (panel *e*). Abbreviations: RCP8.5, Representative Concentration Pathway 8.5; SSP5, Shared Socioeconomic Pathway 5. Panel *a* adapted from Bianchi et al. (2018); panel *c* adapted from Deutsch et al. (2022); panel *e* adapted with permission from Penn & Deutsch (2022); panel *f* adapted with permission from Penn et al. (2018).

consequences for the global nitrogen cycle awaits better representation of these zones and their structure and nitrogen cycling processes in long-term global model simulations.

Warming and O<sub>2</sub> loss have been hypothesized to induce body size reductions among marine animals (Cheung et al. 2012), stirring controversy (Atkinson et al. 2022). Body size impacts both metabolic demand for O<sub>2</sub> and the surface areas through which it can be supplied and thus could adapt to regulate the aerobic balance of organisms. In experimental studies on small invertebrates, intergenerational reductions in body size have been induced through both lower O<sub>2</sub> (Hoefnagel & Verberk 2015) and higher temperature, the latter being a pervasive phenomenon termed the temperature–size rule (Forster et al. 2012, Verberk et al. 2020). The high complexity of O<sub>2</sub> supply surfaces such as gills, among other factors, makes extrapolation to fish and other macrofauna a major challenge. Indeed, the hypothesis has been criticized on the grounds that O<sub>2</sub> supply and demand are likely to remain well matched through ontogenetic growth (Lefevre et al. 2017, Pauly & Cheung 2017). This evolutionary counterargument is qualitatively consistent with the weak variations in  $pO_2^{\text{crit}}$  observed during species ontogeny (Nilsson & Östlund-Nilsson 2008). However, even slight allometric variations in hypoxia tolerance can imply significant potential for adaptive body size variation, since smaller values of  $\varepsilon$  require larger changes in body mass per degree of warming, or temperature–size effect, to counteract an aerobic imbalance (Equation 3).

The observed magnitudes of the temperature–size effect and its variability across the spectrum of temperature and body mass can be reproduced using the thermal and geometric traits of O<sub>2</sub> supply and demand (Deutsch et al. 2022). For small species (~1 g) that form the base of the marine food web, up to 30% reductions in body size are projected by the end of the twentieth century, with spatial variations primarily reflecting the pattern of warming and with regional modulation by O<sub>2</sub> loss (**Figure 7c**). The direction and magnitude of projected size reductions are also broadly consistent with observations in the fossil record. Long-term cooling is associated with increased body size of benthic fauna (e.g., Hunt & Roy 2006) (**Figure 7d**) but is punctuated by body size reductions during intervals of rapid warming (e.g., Kaiho et al. 2006). More detailed applications of such models to paleoclimate records are needed to determine the role of temperature versus  $pO_2$  as the cause of body size change.

While body size reductions predicted by metabolic modeling appear broadly consistent with both experimental and paleontological evidence, there remains substantial uncertainty about the limits to such predictions in larger organisms, where direct empirical tests are scarce. The convergence of allometric scaling of O<sub>2</sub> supply and demand implies that body size ceases to be an effective

adaptation; however, further work is needed to establish the limits of the so-called shrinking-fishes hypothesis. The ability of macrofaunal species to avoid reduced  $\Phi$  by following preferred thermal and aerobic conditions through migration (Pinsky et al. 2020) may reduce the need for such adaptive strategies, but it also implies a wholesale reshuffling of marine communities through shifting range boundaries with widespread local extirpation, colonization, and possible extinction.

If climate warming and ocean  $O_2$  loss push species  $\Phi$  and body sizes beyond their viable ecological limits, then the loss of local aerobic habitat leads to species extirpation. This mechanism explains shifts in the abundance of anchovy populations in the California Current System as a result of natural climate variability (Howard et al. 2020) and may lead indirectly to range expansion of market squid there (Burford et al. 2022).

If enough local habitat disappears, any remaining global habitat may not be sufficient to sustain a viable species population, eventually leading to extinction. Projections of future aerobic habitat changes combining species traits,  $\Phi$ , and a group of Earth system models simulating future climate states indicate that widespread habitat loss could eventually lead to extirpations and global extinctions of many species (Penn & Deutsch 2022) (**Figure 7e**). Despite tropical oxygenation, warming causes local habitat losses to peak in low latitudes where species are living closer to their ecological limits, while model projections reveal that high-latitude species are at a greater risk of global extinction. This latitudinal extinction gradient arises because high-latitude species have nowhere to seek refuge from warm, low- $O_2$  conditions as they become globally widespread, whereas tropical endemics are adapted to such extreme temperatures and  $pO_2$  and counter local habitat loss by colonizing higher latitudes.

The pattern of projected future extinctions mirrors that in paleo simulations of Earth's largest mass extinction, at the end of the Permian (~252 million years ago), which were constrained by the climate warming and widespread  $O_2$  loss implied by geochemical proxies and reproduce the latitudinal extinction gradient observed in the marine fossil record (Penn et al. 2018) (**Figure 7f**). This correspondence supports temperature-dependent hypoxia as the primary cause of the Great Dying in the ocean. Because the greenhouse-gas-driven warming and oceanic  $O_2$  loss differ in magnitude but not in kind, these results support the contention that aerobic habitat loss could also pose a large threat to future marine biodiversity if trends in greenhouse-gas emissions are not rapidly reversed.

#### 4. OUTLOOK AND FUTURE DIRECTIONS

The influence of temperature and oxygen on species biogeography and diversity and their response to climate change is most easily seen at the global scale. However, organisms and populations live in highly heterogeneous environments, under conditions that can vary over distances of meters and over timescales of days or even diurnally, especially in shallow waters. Relationships between large-scale climate dynamics and biogeography offer limited ability to predict the fate of populations at the spatial and temporal scales at which individual organisms navigate the simultaneous constraints of environmental and ecological pressures. These represent major uncertainties for the future and opportunities for further investigations.

The impact of climate on habitability in the ocean, as on land, is exerted in part through the frequency and intensity of extreme conditions. Episodic extremes, the equivalent of ocean weather (Bates et al. 2018), can have a long-lasting influence on populations and thus habitability, even if they occur infrequently. The characterization and consequences of habitat heterogeneity in space and time pose a major scientific challenge for both observations and models. This challenge can be partly addressed through Earth system models, which are increasingly capable of simulating key biotic stressors with high spatial and temporal resolution. Such models suggest

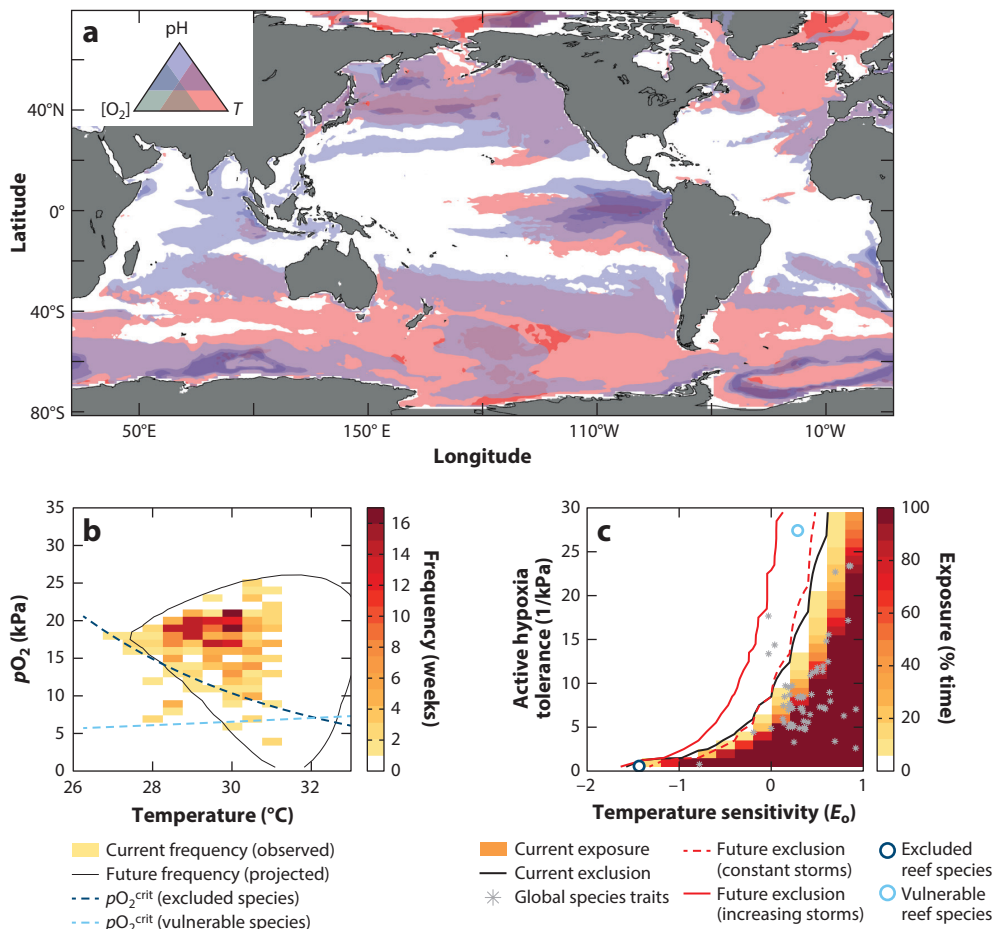


**Figure 8**

From global climate to local weather. (a) Co-occurring extreme conditions throughout the open ocean, shown as the mean intensities of all days when temperature (red), pH (blue), and [O<sub>2</sub>] (green) exceed a fixed relative threshold based on preindustrial reference for all properties in surface water. Compound events (mixed colors) occur in the tropics but underestimate the degree to which they involve low-O<sub>2</sub> extremes. (b) Bivariate frequency distribution of temperature and pO<sub>2</sub> conditions from a decade of weekly measurements on a Caribbean coral reef. The distribution shows an increased frequency and intensity of low O<sub>2</sub> in warmer periods. Active temperature-dependent pO<sub>2</sub><sup>crit</sup> curves are shown for two resident reef invertebrates (navy and light blue dashed lines). (c) Current and projected hypoxia exposure and exclusion thresholds for the reef both with and without the warming-driven increase in O<sub>2</sub> variance. While one hypoxia-tolerant species (light blue circle) currently inhabits the inner reef, its hypoxia exposure is projected to increase due to the increased frequency of metabolic storms, which exceeds the habitable threshold (solid red line) apparent for the more hypoxia-vulnerable species (navy circle). Reef conditions currently preclude habitability for nearly all other species with measured traits (gray asterisks; data also shown in Figure 5b). Abbreviation: pO<sub>2</sub>, O<sub>2</sub> partial pressure. Panel a adapted with permission from Gruber et al. (2021); panels b and c adapted from Lucey et al. (2023) (CC BY 4.0).

that the co-occurrence of extreme low-O<sub>2</sub> and high-temperature conditions are increasing across much of the open ocean (Gruber et al. 2021) (Figure 8a).

Marine heatwaves coupled with episodic extremes of low O<sub>2</sub> constitute a perfect metabolic storm that dramatically, albeit temporarily, erodes aerobic habitability. Detecting such events and their long-term consequences is hampered by the scarcity of hydrographic measurements at high temporal and spatial resolution, especially when coupled with the physiological traits and biogeographic response of species impacted by such storms.

Recent integration of physiological traits, biogeographic field surveys, and high-frequency hydrographic data revealed a key role for such metabolic storms in a well-studied Caribbean coral reef (Lucey et al. 2023). Laboratory experiments on two reef-dwelling brittle star species yielded physiological tolerances and metabolic index traits that are adapted to their warm tropical reef environment that experiences low  $O_2$ . While the reef conditions are on average well within the tolerance limits of both species, the one with lower active hypoxia tolerance is absent from portions of the reef with greater temporal variability. The niche partitioning between the two species arises from the differential effect of metabolic storms on species with distinct traits governing their active and temperature-dependent tolerance to hypoxia.

The frequency and intensity of the reef's metabolic storms have also increased with rising temperatures (Lucey et al. 2023). Extrapolating empirical relationships between temperature and the frequency and intensity of metabolic storms implies that this Caribbean reef will progressively exclude ever more hypoxia-tolerant species, despite the lack of a historical  $pO_2$  trend (Figure 8c). A warming-driven increase in the frequency or intensity of low- $O_2$  extremes could accelerate habitat loss across other tropical marine ecosystems, even if average  $pO_2$  remains constant, as global models project for most tropical areas (Figure 4b). The impact of ocean weather may be particularly important in the context of tropical ecosystems, where climate conditions are relatively stable and animals may be living very close to the edge of their habitable space (Stuart-Smith et al. 2017, Tewksbury et al. 2008).

Evaluating whether the increase in metabolic storms is a widespread phenomenon will require more sustained high-frequency measurements of the covariation between  $O_2$  and temperature and simultaneous knowledge of the temperature-dependent hypoxia tolerances of resident species. Filling these data gaps is essential to establish mechanistic links between the extreme conditions of ocean-weather events and their long-term biological impacts.

The  $O_2$  loss originating from large-scale climate warming will compound direct human impacts on the coastal zone via eutrophication, even in eastern boundary regions where nutrient fluxes from upwelling are naturally high (Dussin et al. 2019, Kessouri et al. 2021). Large-scale modes of climate variability generate  $O_2$  anomalies in the open ocean that eventually arrive in coastal environments, conferring some degree of predictability (Buil & Di Lorenzo 2017). However, processes by which open ocean waters cross the continental shelf break are complex, and the degree to which  $O_2$  anomalies are preserved remains uncertain. Models designed to project global climate change are generally not well suited to investigate coastal processes, such as mesoscale air-sea interaction and benthic-pelagic coupling, that occur on finer scales.

Historical sampling of broad-scale  $O_2$  patterns via measurements made by ships and (increasingly) floats can be difficult to relate to the high-frequency variability of coastal waters that is observed largely through moorings and (increasingly) gliders. For example, in the locations where hypoxic mass mortality events have been reported (Figure 1a), the minimum historical  $O_2$  levels from the nearest sites in the largest global database (the World Ocean Database) show  $O_2$  typically in excess of 100  $\mu M$ . In both modeling and empirical analysis, the mismatch between scales remains a major hurdle, and synthesis of datasets allowing large-scale change to be seamlessly linked to local coastal manifestations of hypoxia is urgently needed.

In addition to high-frequency spatiotemporal variability, ecological and evolutionary pressures have the potential to modify trait-based projections of aerobic habitat loss due to the combined imbalance of  $O_2$  supply and demand at individual to global scales (Figure 9). Changes in marine diversity in response to temperature and  $O_2$  have generally assumed fixed traits and environmental niches among diverse but noninteracting species (Figure 9a,b). While such models have had success in reproducing large-scale patterns in the current and past ocean (Figure 8), they represent limited ecological and evolutionary processes, through static rather than dynamic

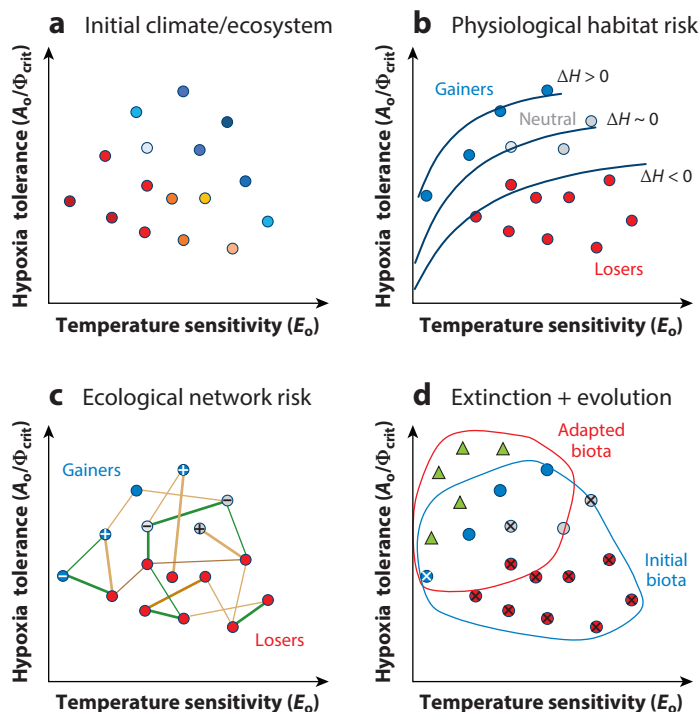


**Figure 9**

From species to ecosystems. (a) How multiple traits govern initial biogeographic distributions. The circle colors represent ranges of initial habitat size, from small (red) to large (blue). (b) How multiple traits govern the gain or loss of habitat ( $\Delta H$ ) from climate warming and  $O_2$  loss. Circle colors indicate whether species gain habitat (blue), lose habitat (red), or experience no change in habitat (gray). (c) How an ecological network can amplify or attenuate the climate impact via species interactions. Line weights indicate the strength of an ecological interaction, and line colors indicate whether an interaction is mutualistic (green) or antagonistic (gold). Plus and minus signs denote where ecological interactions preserve and eliminate species, respectively. (d) How selective pressures lead to the evolution of new species with traits that are well adapted to warmer and less oxygenated environments. Xs indicate species that have gone extinct, and green triangles indicate newly evolved species. Figure adapted with permission from Payne et al. (2023).

ecophysiological parameters. In particular, they provide limited insight into how species responses will cause cascading ecological effects that restructure food webs (Figure 9c) or how trait adaptation might facilitate evolutionary escape from some of the long-term biodiversity losses (Figure 9d). Incorporating ecological and evolutionary dynamics into quantitative trait-based models is, of course, an enormous challenge, but it can be guided by observations already available. Species living in chronically low  $O_2$  provide a glimpse into how traits and ecosystems might adapt to oxygen extremes (Levin 2003, Levin et al. 2009).

As trait-based winners and losers of habitat emerge (Figure 9b), highly tolerant species will fill niches left open by less tolerant species, leading to functional ecosystem changes. Aerobically tolerant species could still be lost if they are ecologically tied to extirpated or vulnerable species through predator–prey, mutualistic, or other critical interactions (Figure 9c). Phenological mismatches, such as misaligned predator–prey resources, can also cause trophic asynchrony (Sydeman et al. 2015). Modeling the impact on ecological networks of differential  $O_2$  sensitivities will require targeted measurements of temperature-dependent hypoxia traits across multiple interacting species and communities.



The changes in ocean biodiversity from loss of  $O_2$ , rising temperature, and related environmental changes are occurring in tandem with massive human interventions in marine ecosystems. The reduced abundance and elevated extinction risk of large-bodied species due to human harvesting pressure are already well documented (Bianchi et al. 2000, Payne et al. 2016) and may be especially severe for top predators with high sensitivity to low  $O_2$  (Prince & Goodyear 2006). The potential for body sizes to decline as an adaptation to warmer and less oxygenated oceans could further compound the size selectivity of direct human interventions. Increased abundances of smaller animals may also be accentuated by the repetitive nature of  $O_2$ -induced extirpations. More than half (54%) of the documented mass mortality events have reoccurred at least once (Figure 1a), resulting in repetitive extirpations with shifts from slow- to fast-growing species (Camillo & Cerrano 2015). The changes in size structure are also tightly coupled to ecosystem simplification (Diaz et al. 2011) (Supplemental Appendix A). This coupling involves the loss of foundation or keystone species, such as oysters and corals, which provide complex structural habitat for fish and other invertebrates and have been identified in nearly half of the recent mass mortality events (Figure 1a). Elimination of these species dramatically alters ecosystem structure and function (Johnson et al. 2021).

Evolutionary responses to intensifying aerobic constraints have the capacity to ameliorate climate-driven imbalances in organismal  $O_2$  supply and demand. However, such processes are generally slow and unpredictable. They are also unlikely to prevent or reverse damage accrued to humans who rely on the ocean directly for their livelihoods and culture. The magnitude of future biotic disruptions arising from anthropogenic climate warming and  $O_2$  reduction depends largely on cumulative greenhouse-gas emissions (Figure 10), but  $O_2$  trends and resulting

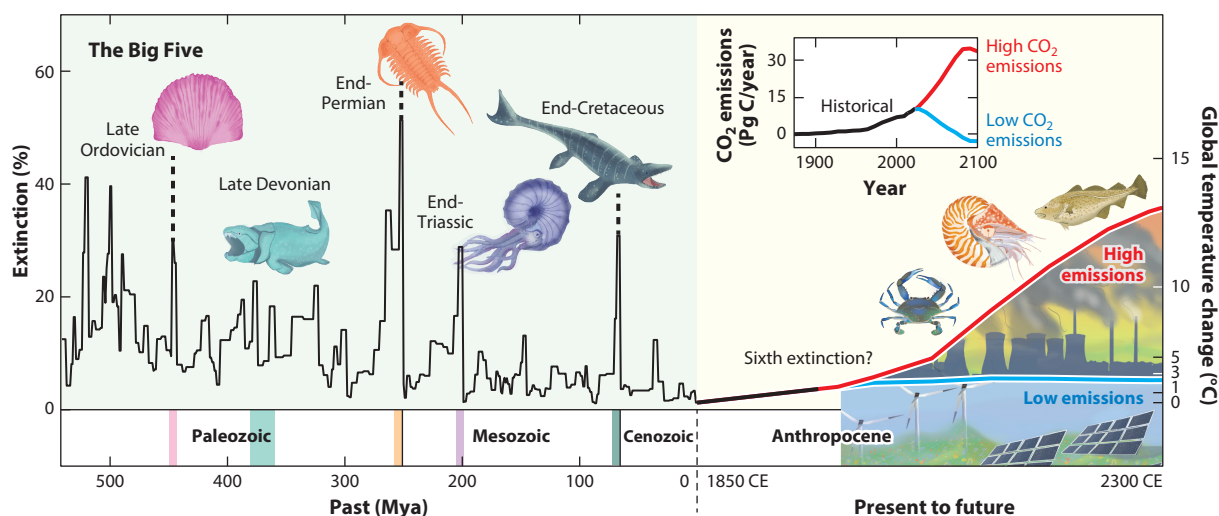


**Figure 10**

Climate pathways to preserve biodiversity. Unchecked climate warming and ocean  $O_2$  loss increase the risk of a sixth mass extinction of life in the oceans. Future extinction risks from climate-driven  $O_2$  imbalances have the potential to rival the past canonical Big Five mass extinctions (labeled) unless trends in greenhouse-gas emissions are rapidly reversed. The future (red and blue lines) is projected using a trait-based aerobic habitat model, the metabolic index ( $\Phi$ ), applied to a group of Earth system model simulations of climate change for the coming centuries under divergent greenhouse-gas-emissions scenarios (inset). The right y axis displays changes in annual mean global surface air temperature for a given magnitude of extinction risk (percentage of model species types lost; left y axis). Note the break in timescale between the past and future. Past extinction levels are based on the percentage of genera lost across 1-million-year intervals from fossil record analyses by Rohde & Muller (2005) (thin black line) and Stanley (2016) (vertical dashed lines) using Sepkoski's *A Compendium of Fossil Marine Animal Genera* (Sepkoski 2002). Figure adapted with permission from Penn & Deutsch (2022) with additional illustrations by Y. Román.

ecosystem responses are likely to continue manifesting well after emissions have declined or stopped (Oschlies 2021). Ocean biodiversity took ~3–5 million years to recover from past mass extinctions (Burgess et al. 2014), illustrating the geologically enduring repercussions of societal choices about climate over the coming decades. It is not too late to reduce CO<sub>2</sub> emissions to avoid the impacts of global O<sub>2</sub> imbalance on global marine biodiversity, but every year of delayed action consigns more ecosystems to disruption and more species to disappearance.

## DISCLOSURE STATEMENT

The authors are not aware of any affiliations, memberships, funding, or financial holdings that might be perceived as affecting the objectivity of this review.

## LITERATURE CITED

- Altieri AH, Harrison SB, Seemann J, Collin R, Diaz RJ, Knowlton N. 2017. Tropical dead zones and mass mortalities on coral reefs. *PNAS* 114(14):3660–65
- Andrews OD, Bindoff NL, Halloran PR, Ilyina T, Le Quéré C. 2013. Detecting an external influence on recent changes in oceanic oxygen using an optimal fingerprinting method. *Biogeosciences* 10(3):1799–813
- Atkinson D, Leighton G, Berenbrink M. 2022. Controversial roles of oxygen in organismal responses to climate warming. *Biol. Bull.* 243(2):207–19
- Auderset A, Moretti S, Taphorn B, Ebner P-R, Kast E, et al. 2022. Enhanced ocean oxygenation during Cenozoic warm periods. *Nature* 609(7925):77–82
- Babbitt AR, Keil RG, Devol AH, Ward BB. 2014. Organic matter stoichiometry, flux, and oxygen control nitrogen loss in the ocean. *Science* 344(6182):406–8
- Bates AE, Helmuth B, Burrows MT, Duncan MI, Garrabou J, et al. 2018. Biologists ignore ocean weather at their peril. *Nature* 560(7718):299–301
- Battye W, Aneja VP, Schlesinger WH. 2017. Is nitrogen the next carbon? *Earth's Future* 5(9):894–904
- Bianchi D, Galbraith ED, Carozza DA, Mislán KAS, Stock CA. 2013. Intensification of open-ocean oxygen depletion by vertically migrating animals. *Nat. Geosci.* 6(7):545–48
- Bianchi D, Weber TS, Kiko R, Deutsch C. 2018. Global niche of marine anaerobic metabolisms expanded by particle microenvironments. *Nat. Geosci.* 11(4):263–68
- Bianchi G, Gislason H, Graham K, Hill L, Jin X, et al. 2000. Impact of fishing on size composition and diversity of demersal fish communities. *ICES J. Mar. Sci.* 57(3):558–71
- Birk MA, McLean EL, Seibel BA. 2018. Ocean acidification does not limit squid metabolism via blood oxygen supply. *J. Exp. Biol.* 221(19):jeb187443
- Boag TH, Stockey RG, Elder LE, Hull PM, Sperling EA. 2018. Oxygen, temperature and the deep-marine stenothermal cradle of Ediacaran evolution. *Proc. R. Soc. B* 285(1893):20181724
- Bohlen L, Dale AW, Wallmann K. 2012. Simple transfer functions for calculating benthic fixed nitrogen losses and C:N:P regeneration ratios in global biogeochemical models. *Glob. Biogeochem. Cycles* 26(3):GB3029
- Boyer TP, Garcia HE, Locarnini RA, Zweng MM, Mishonov AV, et al. 2018. *World Ocean Atlas 2018*. Dataset, Natl. Cent. Environ. Inf., Natl. Ocean. Atmos. Adm., Washington, DC. <https://www.ncei.noaa.gov/access/metadata/landing-page/bin/iso?id=gov.noaa.nodc:NCEI-WOA18>
- Breitbart D, Levin LA, Oschlies A, Grégoire M, Chavez FP, et al. 2018. Declining oxygen in the global ocean and coastal waters. *Science* 359(6371):eaam7240
- Brett JR. 1971. Energetic responses of salmon to temperature. A study of some thermal relations in the physiology and freshwater ecology of sockeye salmon (*Oncorhynchus nerka*). *Am. Zool.* 11(1):99–113
- Buil MP, Di Lorenzo E. 2017. Decadal dynamics and predictability of oxygen and subsurface tracers in the California Current System. *Geophys. Res. Lett.* 44(9):4204–13
- Burford BP, Wild LA, Schwarz R, Chenoweth EM, Sreenivasan A, et al. 2022. Rapid range expansion of a marine ectotherm reveals the demographic and ecological consequences of short-term variability in seawater temperature and dissolved oxygen. *Am. Nat.* 199(4):523–50

- Burgess SD, Bowring S, Shen S. 2014. High-precision timeline for Earth's most severe extinction. *PNAS* 111(9):3316–21
- Buseck JJM, Resplandy L, Ditkovsky SJ, John JG. 2022. Diverging fates of the Pacific Ocean oxygen minimum zone and its core in a warming world. *AGU Adv.* 3(6):e2021AV000470
- Camillo CGD, Cerrano C. 2015. Mass mortality events in the NW Adriatic Sea: phase shift from slow- to fast-growing organisms. *PLOS ONE* 10(5):e0126689
- Chabot D, Steffensen JF, Farrell AP. 2016. The determination of standard metabolic rate in fishes. *J. Fish Biol.* 88(1):81–121
- Chaudhary C, Richardson AJ, Schoeman DS, Costello MJ. 2021. Global warming is causing a more pronounced dip in marine species richness around the equator. *PNAS* 118(15):e2015094118
- Chaudhary C, Saeedi H, Costello MJ. 2017. Marine species richness is bimodal with latitude: a reply to Fernandez and Marques. *Trends Ecol. Evol.* 32(4):234–37
- Cheung WWL, Sarmiento JL, Dunne J, Frölicher TL, Lam VWY, et al. 2012. Shrinking of fishes exacerbates impacts of global ocean changes on marine ecosystems. *Nat. Clim. Change* 3(3):254–58
- Clarke A, Johnston NM. 1999. Scaling of metabolic rate with body mass and temperature in teleost fish. *J. Anim. Ecol.* 68(5):893–905
- Clarke TM, Wabnitz CCC, Striegel S, Frölicher TL, Reygondeau G, Cheung WWL. 2021. Aerobic growth index (AGI): an index to understand the impacts of ocean warming and deoxygenation on global marine fisheries resources. *Prog. Oceanogr.* 195:102588
- Cram JA, Weber T, Leung SW, McDonnell AMP, Liang J-H, Deutsch C. 2018. The role of particle size, ballast, temperature, and oxygen in the sinking flux to the deep sea. *Glob. Biogeochem. Cycles* 32(5):858–76
- Deutsch C, Berelson W, Thunell R, Weber T, Tems C, et al. 2014. Centennial changes in North Pacific anoxia linked to tropical trade winds. *Science* 345(6197):665–68
- Deutsch C, Brix H, Ito T, Frenzel H, Thompson L. 2011. Climate-forced variability of ocean hypoxia. *Science* 333(6040):336–39
- Deutsch C, Ferrel A, Seibel B, Pörtner H-O, Raymond BH. 2015. Climate change tightens a metabolic constraint on marine habitats. *Science* 348(6239):1132–36
- Deutsch C, Penn JL, Seibel B. 2020. Metabolic trait diversity shapes marine biogeography. *Nature* 585(7826):557–62
- Deutsch C, Penn JL, Verberk WCEP, Inomura K, Endress M-G, Payne JL. 2022. Impact of warming on aquatic body sizes explained by metabolic scaling from microbes to macrofauna. *PNAS* 119(28):e2201345119
- DeVries T, Deutsch C. 2014. Large-scale variations in the stoichiometry of marine organic matter respiration. *Nat. Geosci.* 7(12):890–94
- Diaz R, Selman M, Chique C. 2011. *Global eutrophic and hypoxic coastal systems*. Dataset, World Resour. Inst., Washington, DC. <https://datasets.wri.org/dataset/eutrophication-hypoxia-map-data-set>
- Diaz RJ, Rosenberg R. 2008. Spreading dead zones and consequences for marine ecosystems. *Science* 321(5891):926–29
- Duncan MI, James NC, Potts WM, Bates AE. 2020. Different drivers, common mechanism; the distribution of a reef fish is restricted by local-scale oxygen and temperature constraints on aerobic metabolism. *Conserv. Physiol.* 8(1):coaa090
- Dussin R, Curchitser EN, Stock CA, Van Oostende N. 2019. Biogeochemical drivers of changing hypoxia in the California Current Ecosystem. *Deep-Sea Res. II* 169–170:104590
- Endress M-GA, Boag TH, Burford BP, Penn JL, Sperling EA, Deutsch CA. 2022. Physiological causes and biogeographic consequences of thermal optima in the hypoxia tolerance of marine ectotherms. *bioRxiv* 2022.02.03.478967. <https://doi.org/10.1101/2022.02.03.478967>
- Ern R, Norin T, Gamperl AK, Esbaugh AJ. 2016. Oxygen dependence of upper thermal limits in fishes. *J. Exp. Biol.* 219(21):3376–83
- Fennel K, Testa JM. 2019. Biogeochemical controls on coastal hypoxia. *Annu. Rev. Mar. Sci.* 11:105–30
- Forster J, Hirst AG, Atkinson D. 2012. Warming-induced reductions in body size are greater in aquatic than terrestrial species. *PNAS* 109(47):19310–14
- Franco AC, Kim H, Frenzel H, Deutsch C, Ianson D, et al. 2022. Impact of warming and deoxygenation on the habitat distribution of Pacific halibut in the Northeast Pacific. *Fish. Oceanogr.* 31(6):601–14

- Fry FEJ, Hart JS. 1948. The relation of temperature to oxygen consumption in the goldfish. *Biol. Bull.* 94(1):66–77
- Fu W, Primeau F, Moore JK, Lindsay K, Randerson JT. 2018. Reversal of increasing tropical ocean hypoxia trends with sustained climate warming. *Glob. Biogeochem. Cycles* 32(4):551–64
- Gillooly JF, Brown JH, West GB, Savage VM, Charnov EL. 2001. Effects of size and temperature on metabolic rate. *Science* 293(5538):2248–51
- Gillooly JF, Gomez JP, Mavrodiev EV, Rong Y, McLaMORE ES. 2016. Body mass scaling of passive oxygen diffusion in endotherms and ectotherms. *PNAS* 113(19):5340–45
- Giovannoni S, Chan F, Davis E II, Deutsch C, Wolf S. 2021. Biochemical barriers on the path to ocean anoxia? *mBio* 12(4):e01332–21
- Gruber N, Boyd PW, Frölicher TL, Vogt M. 2021. Biogeochemical extremes and compound events in the ocean. *Nature* 600(7889):395–407
- Hammond KA, Diamond J. 1997. Maximal sustained energy budgets in humans and animals. *Nature* 386(6624):457–62
- Hoefnagel KN, Verberk WCEP. 2015. Is the temperature-size rule mediated by oxygen in aquatic ectotherms? *J. Therm. Biol.* 54:56–65
- Howard EM, Penn JL, Frenzel H, Seibel BA, Bianchi D, et al. 2020. Climate-driven aerobic habitat loss in the California Current System. *Sci. Adv.* 6(20):eaay3188
- Hunt G, Roy K. 2006. Climate change, body size evolution, and Cope's Rule in deep-sea ostracodes. *PNAS* 103(5):1347–52
- Ilyina T, Heinze M. 2019. Carbonate dissolution enhanced by ocean stagnation and respiration at the onset of the Paleocene-Eocene Thermal Maximum. *Geophys. Res. Lett.* 46(2):842–52
- IPCC (Intergov. Panel Clim. Change). 2021. *Climate Change 2021: The Physical Science Basis; Contribution of Working Group I to the Sixth Assessment Report of the Intergovernmental Panel on Climate Change*, ed. V Masson-Delmotte, P Zhai, A Pirani, SL Connors, C Péan, et al. Cambridge, UK: Cambridge Univ. Press
- Ito T, Long MC, Deutsch C, Minobe S, Sun D. 2019. Mechanisms of low-frequency oxygen variability in the North Pacific. *Glob. Biogeochem. Cycles* 33(2):110–24
- Ito T, Minobe S, Long MC, Deutsch C. 2017. Upper ocean O<sub>2</sub> trends: 1958–2015. *Geophys. Res. Lett.* 44(9):4214–23
- Ito T, Takano Y, Deutsch C, Long MC. 2022. Sensitivity of global ocean deoxygenation to vertical and isopycnal mixing in an ocean biogeochemistry model. *Glob. Biogeochem. Cycles* 36(4):e2021GB007151
- Johnson MD, Scott JJ, Leray M, Lucey N, Rodriguez Bravo LM, et al. 2021. Rapid ecosystem-scale consequences of acute deoxygenation on a Caribbean coral reef. *Nat. Commun.* 12:4522
- Kaiho K, Takeda K, Petrizzo MR, Zachos JC. 2006. Anomalous shifts in tropical Pacific planktonic and benthic foraminiferal test size during the Paleocene–Eocene thermal maximum. *Palaeogeogr. Palaeoclimatol. Palaeoecol.* 237(2–4):456–64
- Karstensen J, Stramma L, Visbeck M. 2008. Oxygen minimum zones in the eastern tropical Atlantic and Pacific oceans. *Prog. Oceanogr.* 77(4):331–50
- Keeling RF, Körtzinger A, Gruber N. 2010. Ocean deoxygenation in a warming world. *Annu. Rev. Mar. Sci.* 2:199–229
- Kessouri F, McWilliams JC, Bianchi D, Sutula M, Renault L, et al. 2021. Coastal eutrophication drives acidification, oxygen loss, and ecosystem change in a major oceanic upwelling system. *PNAS* 118(21):e2018856118
- Killen SS, Glazier DS, Rezende EL, Clark TD, Atkinson D, et al. 2016. Ecological influences and morphological correlates of resting and maximal metabolic rates across teleost fish species. *Am. Nat.* 187(5):592–606
- Kwiatkowski L, Torres O, Bopp L, Aumont O, Chamberlain M, et al. 2020. Twenty-first century ocean warming, acidification, deoxygenation, and upper-ocean nutrient and primary production decline from CMIP6 model projections. *Biogeosciences* 17(13):3439–70
- Lefevre S, McKenzie DJ, Nilsson GE. 2017. Models projecting the fate of fish populations under climate change need to be based on valid physiological mechanisms. *Glob. Change Biol.* 23(9):3449–59

- Levin LA. 2003. Oxygen minimum zone benthos: adaptation and community response to hypoxia. In *Oceanography and Marine Biology: An Annual Review*, Vol. 41, ed. RN Gibson, RJA Atkinson, pp. 1–45. London: Taylor & Francis
- Levin LA, Ekau W, Gooday AJ, Jorissen F, Middelburg JJ, et al. 2009. Effects of natural and human-induced hypoxia on coastal benthos. *Biogeosciences* 6(10):2063–98
- Levin LA, Liu K-K, Emeis K-C, Breitburg DL, Cloern J, et al. 2015. Comparative biogeochemistry-ecosystem-human interactions on dynamic continental margins. *J. Mar. Syst.* 141:3–17
- Lewis SL, Maslin MA. 2015. Defining the Anthropocene. *Nature* 519(7542):171–80
- Long MC, Deutsch C, Ito T. 2016. Finding forced trends in oceanic oxygen. *Glob. Biogeochem. Cycles* 30(2):381–97
- Long MC, Ito T, Deutsch C. 2019. Oxygen projections for the future. In *Ocean Deoxygenation: Everyone's Problem; Causes, Impacts, Consequences and Solutions*, ed. D Laffoley, JM Baxter, pp. 171–211. Gland, Switz.: Int. Union Conserv. Nat.
- Lucey NM, Deutsch CA, Carignan M-H, Vermandele F, Collins M, et al. 2023. Climate warming erodes tropical reef habitat through frequency and intensity of episodic hypoxia. *PLOS Clim.* 2(3):e0000095
- Marinov I, Gnanadesikan A, Toggweiler JR, Sarmiento JL. 2006. The Southern Ocean biogeochemical divide. *Nature* 441(7096):964–67
- Marquis S. 2022. Stressed out: Dungeness crabs off the Pacific Northwest coast. *National Marine Sanctuaries*. <https://sanctuaries.noaa.gov/news/nov22/stressed-out.html>
- Matear RJ, Hirst AC. 2003. Long-term changes in dissolved oxygen concentrations in the ocean caused by protracted global warming. *Glob. Biogeochem. Cycles* 17(4):1125
- Molina AN, Pulgar JM, Rezende EL, Carter MJ. 2023. Heat tolerance of marine ectotherms in a warming Antarctica. *Glob. Change Biol.* 29(1):179–88
- Nilsson GE, Östlund-Nilsson S. 2008. Does size matter for hypoxia tolerance in fish? *Biol. Rev.* 83(2):173–89
- Oschlies A. 2021. A committed fourfold increase in ocean oxygen loss. *Nat. Commun.* 12:2307
- Oschlies A, Brandt P, Stramma L, Schmidtko S. 2018. Drivers and mechanisms of ocean deoxygenation. *Nat. Geosci.* 11:467–73
- Pan YK, Ern R, Esbaugh AJ. 2016. Hypoxia tolerance decreases with body size in red drum *Sciaenops ocellatus*. *J. Fish Biol.* 89(2):1488–93
- Paulmier A, Ruiz-Pino D. 2009. Oxygen minimum zones (OMZs) in the modern ocean. *Prog. Oceanogr.* 80(3–4):113–28
- Pauly D. 2021. The gill-oxygen limitation theory (GOLT) and its critics. *Sci. Adv.* 7(2):eabc6050
- Pauly D, Cheung WWL. 2017. Sound physiological knowledge and principles in modeling shrinking of fishes under climate change. *Glob. Change Biol.* 24(1):e15–26
- Payne JL, Al Aswad JA, Deutsch C, Monarrez PM, Penn JL, Singh PK. 2023. Selectivity of mass extinctions: patterns, processes, and future directions. *Camb. Prisms Extinctions* 1:E12
- Payne NL, Smith JA, van der Meulen DE, Taylor MD, Watanabe YY, et al. 2016. Temperature dependence of fish performance in the wild: links with species biogeography and physiological thermal tolerance. *Funct. Ecol.* 30:903–12
- Penn JL, Deutsch C. 2022. Avoiding ocean mass extinction from climate warming. *Science* 376(6592):524–26
- Penn JL, Deutsch C, Payne J, Sperling E. 2018. Temperature-dependent hypoxia explains biogeography and severity of end-Permian marine mass extinction. *Science* 362(6419):eaat1327
- Penn JL, Weber T, Deutsch C. 2016. Microbial functional diversity alters the structure and sensitivity of oxygen deficient zones. *Geophys. Res. Lett.* 43(18):9773–80
- Pinsky ML, Eikeset AM, McCauley DJ, Payne JL, Sunday JM. 2019. Greater vulnerability to warming of marine versus terrestrial ectotherms. *Nature* 569(7754):108
- Pinsky ML, Selden RL, Kitchel ZJ. 2020. Climate-driven shifts in marine species ranges: scaling from organisms to communities. *Annu. Rev. Mar. Sci.* 12:153–79
- Pitcher GC, Aguirre-Velarde A, Breitburg D, Cardich J, Carstensen J, et al. 2021. System controls of coastal and open ocean oxygen depletion. *Prog. Oceanogr.* 197:102613
- Prince ED, Goodyear CP. 2006. Hypoxia-based habitat compression of tropical pelagic fishes. *Fish. Oceanogr.* 15(6):451–64



- Rogers NJ, Urbina MA, Reardon EE, McKenzie DJ, Wilson RW. 2016. A new analysis of hypoxia tolerance in fishes using a database of critical oxygen level ( $P_{crit}$ ). *Conserv. Physiol.* 4(1):cow012
- Rohde RA, Muller RA. 2005. Cycles in fossil diversity. *Nature* 434(7030):208–10
- Sarmiento JL, Gruber N. 2006. *Ocean Biogeochemical Dynamics*. Princeton, NJ: Princeton Univ. Press
- Schmidtoko S, Stramma L, Visbeck M. 2017. Decline in global oceanic oxygen content during the past five decades. *Nature* 542:335–51
- Schmidt-Nielsen K. 1984. *Scaling: Why Is Animal Size So Important?* Cambridge, UK: Cambridge Univ. Press
- Seibel BA. 2011. Critical oxygen levels and metabolic suppression in oceanic oxygen minimum zones. *J. Exp. Biol.* 214(2):326–36
- Sepkoski JJ. 2002. *A Compendium of Fossil Marine Animal Genera*. Ithaca, NY: Paleontol. Res. Inst.
- Shepherd JG, Brewer PG, Oschlies A, Watson AJ. 2017. Ocean ventilation and deoxygenation in a warming world: introduction and overview. *Philos. Trans. R. Soc. A* 375(2102):20170240
- Sperling EA, Boag TH, Duncan MI, Endriga CR, Marquez JA, et al. 2022. Breathless through time: oxygen and animals across Earth's history. *Biol. Bull.* 243(2):184–206
- Sperling EA, Frieder CA, Levin LA. 2016. Biodiversity response to natural gradients of multiple stressors on continental margins. *Proc. R. Soc. B* 283(1829):20160637
- Stanley S. 2016. Estimates of the magnitudes of major marine mass extinctions in earth history. *PNAS* 113(42):E6325–34
- Stramma L, Oschlies A, Schmidtoko S. 2012. Mismatch between observed and modeled trends in dissolved upper-ocean oxygen over the last 50 yr. *Biogeosciences* 9(10):4045–57
- Stuart-Smith RD, Edgar GJ, Bates AE. 2017. Thermal limits to the geographic distributions of shallow-water marine species. *Nat. Ecol. Evol.* 1(12):1846–52
- Sydeman WJ, Poloczanska E, Reed TE, Thompson SA. 2015. Climate change and marine vertebrates. *Science* 350(6262):772–77
- Terada M, Minobe S, Deutsch C. 2019. Mechanisms of future changes in equatorial upwelling: CMIP5 intermodel analysis. *J. Clim.* 33(2):497–510
- Tewksbury JJ, Huey RB, Deutsch CA. 2008. Putting the heat on tropical animals. *Science* 320(5881):1296–97
- Tittensor DP, Mora C, Jetz W, Lotze HK, Ricard D, et al. 2010. Global patterns and predictors of marine biodiversity across taxa. *Nature* 466(7310):1098–101
- Vaquier-Sunyer R, Duarte CM. 2008. Thresholds of hypoxia for marine biodiversity. *PNAS* 105(40):15452–57
- Verberk WCEP, Atkinson D, Hoefnagel KN, Hirst AG, Horne CR, Siepel H. 2020. Shrinking body sizes in response to warming: explanations for the temperature-size rule with special emphasis on the role of oxygen. *Biol. Rev. Camb. Philos. Soc.* 96(1):247–68
- Weber T, Deutsch C. 2012. Oceanic nitrogen reservoir regulated by plankton diversity and ocean circulation. *Nature* 489(7416):419–22
- Wishner KF, Seibel BA, Roman C, Deutsch C, Outram D, et al. 2018. Ocean deoxygenation and zooplankton: Very small oxygen differences matter. *Sci. Adv.* 4(12):eaau5180
- Yasuhara M, Wei C-L, Kucera M, Costello MJ, Tittensor DP, et al. 2020. Past and future decline of tropical pelagic biodiversity. *PNAS* 117(23):12891–96
- Zakem EJ, Follows MJ. 2017. A theoretical basis for a nanomolar critical oxygen concentration. *Limnol. Oceanogr.* 62(2):795–805
- Zhang X, Ward BB, Sigman DM. 2020. Global nitrogen cycle: critical enzymes, organisms, and processes for nitrogen budgets and dynamics. *Chem. Rev.* 120(12):5308–51